

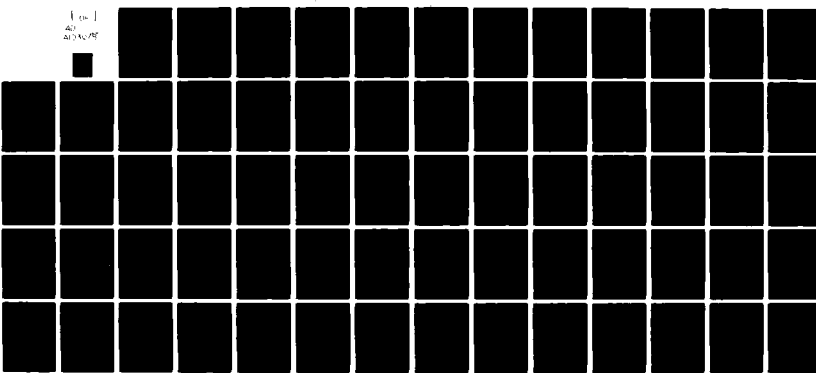
AD-A103 078

GEORGIA INST OF TECH ATLANTA CENTER FOR THE ADVANCEMENT--ETC F/6 20/11  
NUMERICAL ANALYSIS OF DYNAMIC CRACK PROPAGATION: GENERATION AND--ETC(U)  
JUL 81 T NISHIOKA, S.N. ATLURI  
N00014-78-C-0636

UNCLASSIFIED

NL

100-1  
40  
4034, 198



END  
DATE FILMED  
9-81  
DTIC

AD A103078

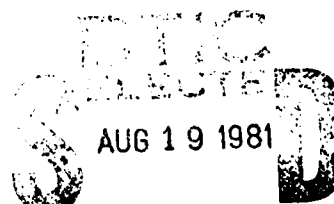
Office of Naval Research  
Contract N00014-78-C-0636 NR 064-610  
Technical Report No. 11  
Report No. GIT-CACM-SNA 9

NUMERICAL ANALYSIS OF DYNAMIC CRACK PROPAGATION: GENERATION  
AND PREDICTION STUDIES

BY

T. Nishioka and S.N. Atluri

*July 1981*



A

Approved for public release and unlimited  
distribution; its  
distribution is unlimited.

Center for the Advancement of Computational Mechanics  
School of Civil Engineering  
Georgia Institute of Technology  
Atlanta, Georgia 30332

81 8 18 075

FILE COPY

A

NUMERICAL ANALYSIS OF DYNAMIC CRACK PROPAGATION: GENERATION  
AND PREDICTION STUDIES

T. Nishioka\* and S.N. Atluri\*\*

Center for the Advancement of Computational Mechanics  
School of Civil Engineering  
Georgia Institute of Technology, Atlanta, Ga. 30332

Abstract:

Results of "generation" (determination of dynamic stress-intensity factor variation with time, for a specified crack-propagation history) studies, as well as "prediction" (determination of crack-propagation history for specified dynamic fracture toughness versus crack-velocity relationships) studies of dynamic crack propagation in plane-stress/strain situations are presented and discussed in detail. These studies were conducted by using a transient finite element method wherein the propagating stress-singularities near the propagating crack-tip have been accounted for. Details of numerical procedures for both the generation and prediction calculations are succinctly described. In both the generation and prediction studies, the present numerical results are compared with available experimental data. It is found that the important problem of dynamic crack propagation prediction can be accurately handled with the present procedures.

Introduction:

For dynamic crack propagation in finite elastic bodies, the interaction with the crack-tip of stress waves reflected from the boundaries and/or emanated by the other moving crack-tip plays an important role in determining the inten-

\*Research Scientist II; \*\* Regents' Professor of Mechanics

sity of the dynamic singular stress-field at the considered crack-tip. Because of the analytical intractability of such elasto-dynamic crack-propagation problems, computational techniques are mandatory. A critical appraisal of several such computational techniques was made by Kanninen [1] in 1978. Most of the finite element techniques reviewed in [1] use conventional assumed displacement finite elements near the crack-tip and hence do not account for the known crack-tip singularity. Moreover in these techniques, crack-propagation was simulated by the well-known "node release" technique, which, as discussed in [1], may not be sufficiently accurate. The literature on dynamic finite element methods for simulation of fast fracture, since the appearance of [1], has been reviewed in [2,3,4].

In Refs. [2,3,4], the authors have presented a "translating-singularity" finite element procedure for simulation of fast crack propagation in finite bodies. In this procedure, a singular-element, wherein the analytical eigen functions for a propagating crack in an infinite domain were used as basis functions for assumed displacements, was used near the crack-tip. In simulating crack-propagation, this singular element was translated by an arbitrary amount  $\Delta\Sigma$  in each time-increment  $\Delta t$  of the time-integration scheme. During this translation, the crack-tip retains a fixed location within the singular element; however, the regular isoparametric elements surrounding the moving singular element deform appropriately. It was shown [2,3,4] that the above finite element method, which was based [2,3] on an energy-consistent variational principle for bodies with changing internal boundaries, leads to a direct evaluation of dynamic K-factors for propagating cracks. Attempts at simplifying the above procedure, by employing alternatively, a singular element with only the well-known Williams' eigen-functions for a stationary crack being used as element basis-functions, or distorted triangular isoparametric elements (the so-called "quarter-point elements"), in place of the above described singular-ele-

ment, were made in [5]. However, all the examples presented in [2-5] fall into the category of "generation studies" in the sense described earlier. Specifically, results for finite-domain counterparts of the well-known analytical problems for infinite domains, solved by Broberg, Freund, Nillsson, Thau and Lui, Sih et al (as referenced in [2,3]), were presented in [2-5], to indicate the effects of finite boundaries, and stress-wave interactions, on dynamic crack-tip stress-intensity, in these problems.

In the present paper, which emphasises the "inverse" or "prediction" problem, namely the determination of crack-tip propagation history in a plane stress/strain problem for a specified dynamic fracture-toughness versus crack-velocity relation, the following topics are discussed: (i) a synopsis of the mathematical formulation for analysis of the "generation" problem; (ii) description of the details of analysis of the "prediction" problem; (iii) detailed description and discussion of the numerical results of both the "generation" and "prediction" studies of wedge-loaded rectangular double cantilever, and tapered double cantilever, beam specimens for which experimental data has been reported by Kalthoff et al [6,7] and independent numerical results have been reported by Kobayashi et al [8], and Popelar and Gehlen [9]. The present paper ends with some conclusions and a discussion of the open questions in numerical analysis of fast crack propagation in realistic metallic structures.

#### Synopsis of the Formulation of "Generation" Problem:

Consider two instants of time  $t_1$  and  $t_2 = t_1 + \Delta t$ . Assuming, without loss of generality, that the crack propagation is in pure mode I, let the crack lengths at  $t_1$  and  $t_2$  be  $\Sigma_1$  and  $\Sigma_2 = \Sigma_1 + \Delta\Sigma$ , respectively. Let the displacements, strains, and stresses at  $t_1$  and  $t_2$  be, respectively,  $(u_i^1, \epsilon_{ij}^1, \sigma_{ij}^1)$ , and  $(u_i^2, \epsilon_{ij}^2, \sigma_{ij}^2)$ . The variables at time  $t_1$  are presumed known. It has been shown [2,3] that the variational principle governing the dynamic crack propagation between  $t_1$  and  $t_2$  can be written as:

$$\begin{aligned}
& \int_{V_2} \{(\sigma_{ij}^2 + \sigma_{ij}^1) \delta \epsilon_{ij}^2 + \rho (\dot{u}_i^2 + \dot{u}_i^1) \delta u_i^2\} dV \\
&= \int_{S_{\sigma 2}} (\bar{T}_i^2 + \bar{T}_i^1) \delta u_i^2 ds + \int_{\Sigma_1^+} (\bar{T}_i^2 + \bar{T}_i^1)^+ (\delta u_i^2)^+ ds \\
&+ \int_{\Delta \Sigma^+} (\bar{T}_i^2 + \sigma_{ij}^1 v_j^1)^+ (\delta u_i^2)^+ ds
\end{aligned} \tag{1}$$

In the above,  $V_2$  is the domain, and  $S_{\sigma 2}$  the external boundary where time-dependent tractions are prescribed, at time  $t_2$ ;  $\bar{T}_i^1$  are the prescribed tractions at time  $t_1$  at  $S_{\sigma 1} (\approx S_{\sigma 2})$  as well as at  $\Sigma_1^+$ ;  $\bar{T}_i^2$  are the prescribed tractions at time  $t_2$  at  $S_{\sigma 2}$  as well as at  $\Delta \Sigma^+$ ;  $(\cdot)^+$  indicates the upper half of the crack face, which only is considered in the present mode I problem. It is seen that  $\sigma_{ij}^1 v_j^1$  are the cohesive forces holding the crack-faces together at time  $t_1$ . Thus, it is seen that the integrand  $(\sigma_{ij}^1 v_j^1)^+ (\delta u_i^2)^+$  in the last term of the r.h.s. of Eq. (1) corresponds to the term of energy-release rate due to dynamic crack propagation. The Eq. (1) may thus be viewed as a virtual energy-balance relation for dynamic crack-propagation, and hence the present numerical method based on Eq. (1) is inherently energy-consistent.

In Eq. (1),  $(u_i^1, \sigma_{ij}^1)$  are known, while  $(\sigma_{ij}^2, \epsilon_{ij}^2)$ , and  $u_i^2$  are the variables. Now, Eq. (1) is used to develop a finite element approximation at time  $t_2$ . Thus, the domain  $V_2$  is discretized into a finite number of elements, with a domain  $V_s$  immediately surrounding the crack-tip being treated as the so-called "singular element", and the domain  $V_2 - V_s$  being mapped by the well-known, 8-noded, isoparametric elements. In the singular-element  $V_s$ , the basis functions for assumed displacements are the crack-velocity dependent eigen-function solutions to the elasto-dynamic problem of crack-propagation in an infinite domain, as discussed in this paper.

Note that at time  $t_2$ , in the present mode I problem, the crack tip is located at  $x_1 = \Sigma_1 + \Delta \Sigma$  and hence the singular-element is centered at  $x_1 = \Sigma_1 + \Delta \Sigma$ . In developing the equations for the finite element mesh at  $t_2$ , it is seen from Eq. (1) that the variation of  $\sigma_{ij}^1$  and  $u_i^1$  must be known in the finite element mesh

at  $t_2$ . However,  $\sigma_{ij}^1$ ,  $u_j^1$ , and  $u_j^1$  were solved for, in the finite element mesh at  $t_1$ . In the mesh at  $t_1$  the crack-tip was located at  $x_1 = \Sigma_1$  and hence the crack element was centered at  $\Sigma_1$ . Thus between  $t_1$  and  $t_2$  ( $t_1 + \Delta t$ ) the crack element is translated by an amount  $\Delta \Sigma$ . While the crack-element is translated, only the elements surrounding the moving crack-tip are distorted. Thus the finite element meshes at times  $t_1$  and  $t_2$  differ only in the location of the crack-tip (and hence the crack-element) and the shapes of the immediately surrounding isoparametric elements. Thus, the known data at  $\sigma_{ij}^1$  and  $u_j^1$  in the mesh at  $t_1$  is interpolated easily into corresponding data in the mesh at  $t_2$ . Further details of the above translating-singularity-element method of simulating dynamic crack propagation in arbitrary shaped finite bodies can be found in [2,3].

We now remark briefly on the basis functions for assumed displacements used in the singular element. Let  $x_\alpha$  ( $\alpha=1,2$ ) be fixed rectangular coordinates in the plane of the present 2-dimensional elastic body, with the crack-tip moving along the  $x_1$  axis and  $x_2$  is normal to the crack-axis. We introduce a coordinate system  $(\xi, x_2)$  which remains fixed w.r.t. the propagating crack-tip, such that  $\xi = x_1 - vt$ , where  $v$  is, without loss of generality, the constant speed of crack-propagation. It can be shown [2,3] that the elastodynamic equations, governing this problem, for the wave potentials  $\phi$  (dilatational) and  $\psi$  (shear) are:

$$[1 - (v/c_d)^2] (\partial^2 \phi / \partial \xi^2) + (\partial^2 \phi / \partial x_2^2) = -(2v/c_d^2) (\partial^2 \phi / \partial t \partial \xi) + (1/c_d^2) (\partial^2 \phi / \partial t^2) \quad (2)$$

and a similar equation for  $\psi$ , except that  $c_d$  in Eq. (2) is to be replaced by  $c_s$ , where  $c_d$  and  $c_s$  are the dilatational and shear wave speeds respectively. The "steady-state" eigen-function solution to the homogeneous part of Eq. (2), namely, the solution which appears time-invariant to an observer moving with the crack-tip, and satisfies the prescribed traction conditions on the crack face ( $\xi < 0$ ,  $x_2 = 0$ ) can be derived easily, as indicated in [2] and elsewhere. We use these eigen function solutions for an infinite body, as basis functions for assumed

displacements within the "crack-tip-singularity-element". However to satisfy the full Eq. (2), the undetermined coefficients,  $\beta_j$  below, in the eigen function expansion are taken to be functions of time. Thus, within the singular element,

$$u_\alpha(\xi, x_2, t) = u_{\alpha j}(\xi, x_2, v) \beta_j(t) \quad [\alpha=1,2; j=1,2..N] \quad (3)$$

where  $u_{\alpha j}$  are the above described eigen-functions, and  $\beta_j$  are undetermined parameters, which are to be determined from the finite element equations for the cracked body.

As seen from Eq. (3), the eigen functions  $u_{\alpha j}$  depend on the crack-tip velocity. In the present numerical approach, the crack-tip velocity is assumed to be constant within each time-increment  $\Delta t$ , say  $v_1$  between  $t_1$  and  $t_1 + \Delta t$ , and  $v_2$  between  $t_2$  and  $t_2 + \Delta t$ , etc. Thus, between  $t_1$  and  $t_1 + \Delta t$ , the eigen-functions embedded in the singularity-element correspond to velocity  $v_1$  and those between  $t_2$  and  $t_2 + \Delta t$  correspond to velocity  $v_2$ . Thus, the present finite element method is capable of handling non-uniform-velocity crack propagation.

The total velocities and accelerations of a material particle in the singular element, within each time step, corresponding to Eq. (3), can be written as:

$$\dot{u}_\alpha = u_{\alpha j} \ddot{\beta}_j - v u_{\alpha j, \xi} \dot{\beta}_j \quad (4)$$

and

$$\ddot{u}_\alpha = u_{\alpha j} \ddot{\beta}_j - 2v u_{\alpha j, \xi} \dot{\beta}_j + v^2 u_{\alpha j, \xi \xi} \beta_j \quad (5)$$

where  $(\cdot)_\xi = \partial(\cdot)/\partial\xi$ , and  $(\dot{\cdot})$  implies a time derivative.

The salient features, pertinent to the studies reported in this paper, of the present method, the mathematical details of which are reported elsewhere [2,3], are as follows:

(i) The eigen functions  $u_{\alpha 1}$  ( $\alpha=1,2$ ) lead to the familiar  $(1/\sqrt{r})$  singularities in strains and stresses. Thus the coefficient  $\beta_1(t)$  is directly related (to within a scalar constant) to the dynamic stress intensity factor,  $K_I(t)$ .

(ii) The compatibility of displacements, velocities, and accelerations of material particles at the boundary of surrounding elements with those of the surrounding (usual) isoparametric elements is satisfied through a continuous least squares approach. If the displacements, velocities, and accelerations of the nodes at the boundary of the singular-element,  $v_s$ , are  $q$ ,  $\dot{q}$ , and  $\ddot{q}$  respectively, the above least-squares technique leads to linear algebraic relations between the sets  $(q, \dot{q}, \ddot{q})$  and  $(\beta, \dot{\beta}, \ddot{\beta})$  where  $\beta$  are undetermined parameters in the eigen-function expansion, Eq. (3), in the singular-element. From these equations and the final finite element equations governing the nodal displacements, velocities, and accelerations of the cracked structure, the variables  $\beta, \dot{\beta}, \ddot{\beta}$  can be computed directly. Thus, the dynamic stress-intensity factor, as well as its first two time derivatives, are computed directly in the present procedure.

(iii) The "transient" finite element equations are integrated in time, using the well-known Newmark's  $\beta$ -method [2,3].

(iv) Because of the use of the eigen functions in a moving coordinate system, as in Eq. (3), in the singular-element, there is the presence of an "apparent" damping matrix for the singular element. Further, for the same reason, this damping matrix as well as the stiffness matrix of the singular-element, are unsymmetric. However, the stiffness and mass matrices of the surrounding isoparametric elements are, of course, symmetric. Thus the final finite element equation system will have a "small" degree of unsymmetry. This equation system is solved, in the present studies, using a simple iterative scheme.

Details of Analysis of Prediction Problem:

The problem here is to predict the time histories of crack-length  $[\Sigma(t)]$ , crack-velocity  $[\dot{\Sigma}(t) \cdot v(t)]$ , and possible crack-arrest, for a specified relationship of dynamic fracture toughness  $[K_{ID}]$  versus crack-velocity  $[v]$ . Until very recently, it was presumed that the relationship  $K_{ID}$  versus  $v$  was a unique

material property. Recently, however, this presumption was brought to question as discussed in [10], due to the apparent geometry and load-rate dependence of the dynamic fracture toughness. A slight specimen-geometry dependence of dynamic fracture toughness versus crack-velocity relationship was noted in the experimental results of Kalthoff et al [6,7]. Kanninen et al[10] also found that dynamically initiated (impact loading) dynamic crack-propagation and quasi-statically initiated dynamic crack propagation, apparently are characterized by markedly different toughness properties. Ways out of this apparent impasse that have been suggested include: (i) to postulate the dependence of dynamic fracture toughness on second (acceleration) and higher-order time derivatives of the crack-length and (ii) considerations of nonlinear effects near the crack-tip, such as plasticity.

The problems considered in the present paper, however, may be argued to fall into the realms of linear elasto-dynamics. Experimental specimens for which the present analysis is applied, made of Araldite B used by Kalthoff et al [7] may be considered to be effectively linear-elastic, even though secondary effects due to rate-dependent viscoelastic properties of the specimen may be present. In any event, the present numerical results and their comparison with the experimental data may effectively serve to check the reasonableness of this approximation. Further, the presented analysis procedure can easily be extended to account for any postulated dependence of dynamic fracture toughness on crack-tip acceleration and/or other higher order time derivatives of crack length, ie when  $K_{ID} = K_{ID}(\ddot{\Sigma}, \ddot{\Sigma}, \ddot{\Sigma}, \dots)$ .

With this motivation, we present some details of analysis of the prediction problem when the fracture toughness relation is given in the form  $K_{ID} = K_{ID}(\Sigma)$ . Thus, this analysis cannot, inherently, either add to or lessen the controversy surrounding the specimen geometry dependence of  $K_{ID}$ .

Let the prediction problem be considered to have been solved upto time  $t_1$ .

In order to find the solution at  $t_2 (\equiv t_1 + \Delta t)$ , the crack-velocity at  $t_2$ , namely,  $v_2 (\equiv \dot{\Sigma}(t_2))$  must be found. To this end, it is first noted that the dynamic stress-intensity factor can be written as:

$$K_I = K_I(t, v) \quad (6)$$

Since, in the present procedure, the velocity of crack-propagation is assumed to be constant within each time-step, an approximate procedure to predict the velocity at  $[t_1 + (\Delta t)/2]$  will be sought. Using double Taylor series expansion, it is seen from Eq. (6) that:

$$K_{Ip}(t_1 + \frac{\Delta t}{2}; v_1 + \Delta v) = \sum_{n=0}^{\infty} \frac{1}{n!} \left\{ \left( \frac{\Delta t}{2} \right) \frac{\partial}{\partial t} + \Delta v \frac{\partial}{\partial v} \right\}^n K_I(t, v) \Big|_{t_1, v_1} \quad (7)$$

where  $K_{Ip}$  is the predicted value of  $K_I$  at  $t_1 + (\Delta t/2)$ . One can, upon expanding terms, write Eq. (7) as:

$$\begin{aligned} K_{Ip} &= K_I(t_1, v_1) + \left( \frac{\Delta t}{2} \right) \dot{K}_I(t_1, v_1) + \frac{1}{2} \left( \frac{\Delta t}{2} \right)^2 \ddot{K}_I(t_1, v_1) + R \\ &\equiv \beta_1(t_1) + \left( \frac{\Delta t}{2} \right) \dot{\beta}_1(t_1) + \frac{1}{2} \left( \frac{\Delta t}{2} \right)^2 \ddot{\beta}_1(t_1) + R \equiv K_{Ip}^* + R \end{aligned} \quad (8)$$

where,  $(\cdot) = \partial(\cdot)/\partial t$ , and  $R$  is "residue" of the Taylor expansion indicated in Eq. (8). Note that use is made of the salient feature of the present analysis procedure, that  $\beta_1(t) \equiv K_I(t)$ ,  $\beta_1$  being the coefficient of the first eigen-functions as in Eq. (3).

Since during dynamic crack propagation,  $K_I = K_{ID}$ , using the predicted  $K_{Ip}$  of Eq. (8) and the specified  $K_{ID}$  versus  $\dot{\Sigma}(t)$  relation, the crack velocity  $v (\equiv \dot{\Sigma})$  at the time  $[t_1 + (\Delta t/2)]$  can be predicted. If the arrest dynamic-toughness is  $K_{ID}^{arr}$ , crack-arrest is predicted if  $K_{Ip} \leq K_{ID}^{arr}$ . Thus, in the present procedure, crack arrest is predicted as a terminal event, if any, in the propagation analysis.

Using the above predicted crack-velocity value, the finite element system of equations at time  $t_2$ , based on Eq. (1), are constructed, and, from these, the actual dynamic stress-intensity factor  $K_I(t_2) [ \equiv \beta_1(t_2) ]$  is computed. Thus, the actual  $K_I$  at  $t_1 + (\Delta t/2)$  is computed, as;

$$K_I(t_1 + \frac{\Delta t}{2}) \approx (1/2)[K_I(t_1) + K_I(t_2)] \quad (9)$$

The correlation between the predicted  $K_{Ip}$  of Eq. (8) and the actual  $K_I$  of Eq. (9) can be seen to depend on the residue, "R", of Eq. (8). To ensure this correlation, a further approximation is introduced in the present work that the residue  $R$  at  $t_1 + (\Delta t/2)$  can be approximated by its known value at  $[t_1 - (\Delta t/2)]$ , in the generic sense.<sup>1)</sup> Thus, in the present procedure, the generic algorithm used to find  $K_{Ip}$  at  $t_1 + (\Delta t/2)$  can be written as:

$$K_{Ip}(t + \frac{\Delta t}{2}) = \beta_1(t_1) + (\frac{\Delta t}{2})^2 \dot{\beta}(t_1) + \frac{1}{2}(\frac{\Delta t}{2})^2 \ddot{\beta}_1(t_1) - [K_I(t_1 - \frac{\Delta t}{2}) - K_{Ip}^*(t_1 - \frac{\Delta t}{2})] \quad (10)$$

In all the presently reported computations, when Eq. (8) with  $R=0$  was used, a maximum error of the order of 3% between  $K_{Ip}$  and  $K_I$  was noted. However, Eq. (10) was used, this maximum error reduced to the order of 0.5%.

We now discuss the "generation" and "propagation" calculations performed on rectangular as well as tapered double cantilever beam specimens of Araldite B materials. The results are compared with the corresponding experimental results reported by Kalthoff et al [6,7], and pertinent conclusions are drawn.

#### Generation Calculations:

To demonstrate the "generation" type calculations, we first treat a wedge-loaded rectangular double cantilever beam specimen (WL-RDCB), the crack-propagation histories and dynamic stress-intensity factor histories in which were directly measured by Kalthoff et al [6]. The relevant geometric data of the WL-RDCB specimen are indicated in Fig. 1 which also shows the finite element model wherein the moving-singularity-element is shown hatched, at the beginning of crack propagation. The material constants used in the present analysis are:  $E=3380 \text{ MN/m}^2$  and Poisson's ratio,  $\nu=0.33$ . In the experiments of [6], several test specimens,

1) As can be expected from Eq. (1), inherent numerical errors (usually, very small) in the present formulation are oscillatory in nature [5]. Thus  $R(+-\Delta t/2)$  is approximated by  $-R(t-\Delta t/2)$ .

wherein cracks were initiated from blunted notches with crack-propagation initiation stress-intensity factors  $K_{Iq}$  larger than the fracture toughness  $K_{Ic}$ , were studied.

Note that the actual loading mechanism in the experiment is closer, in numerical simulation, to loading the finite element model at point A in Fig. 1, with the material to the left hand side of line BA in Fig. 1 also considered to be participating in the motion. In the first attempt at the analysis, however, the loading was modeled to act at point B in Fig. 1 instead, and the material to the left of line AB was not modeled. In the remainder of the paper, the numerical model wherein load was applied at point A of Fig. 1 and the material to the left of line AB (Fig. 1) was also modeled, is often referred to as the "actual loading condition", and the other one as the "simplified loading condition", respectively.

In their report, Kalthoff et al [6] identify the RDCB specimens with  $K_{Iq}$  values  $2.32 \text{ MN/m}^{3/2}$  and  $1.33 \text{ MN/m}^{3/2}$ , respectively, as specimens No. 4 and 17. For convenience, the same identification is used in the presently reported numerical simulation.

As noted earlier, the "generation" calculation used as input, the experimentally measured crack length (and hence crack-velocity) history. The output of the calculation is the directly computed dynamic stress-intensity factor at the tip of the propagating crack for various time instants.

Fig. 2 shows the considered crack velocity and length history for RDCB specimen 4 as reported in [6]. Fig. 2 also shows the presently computed dynamic  $K_I$  as a function of time, along with comparison experimental results of [6], and numerical results of Kobayashi [8]. The present calculation for  $K_I$  was performed in 3 alternate ways: (i) direct computation, since  $K_I$  is same as the undetermined parameter  $\beta_1$  in the element basis functions as mentioned

earlier, (ii) from a crack-tip integral which gives directly the crack-opening energy, and using the crack-velocity dependent relation between  $K_I$  and the energy-release rate, and (iii) calculating fracture energy from a global energy balance relation. It is seen that all the 3 values agree excellently, thus pointing to the inherent consistency of the present numerical procedure. It should be pointed out that the results in Fig. 2 were based on using the forementioned "simplified loading condition". As seen from Fig. 2, the present numerical results, as well as those of Kobayashi [8], exhibit a pronounced peak as compared to the experimental results, even though the peak occurs much later in the present results as compared to those of Kobayashi [8].

Fig. 3 shows variation of different energy quantities: input energy (W); kinetic energy (T); strain energy (U); and fracture energy (F), for RDCB specimen 4, when the "simplified loading condition" is used. It should be noted that in the present procedure, each of the quantities W, T, U, and F is calculated separately and directly. Thus, the fact that  $U+T+F$  is equal to W at all times (no other energy dissipation mechanisms are accounted for here) is an inherent check on the accuracy of the calculation. That this is so can be seen from Fig. 3.

The Fig. 4 demonstrates the effects of the alternate loading-conditions employed in the finite element model of RDCB specimen 4. In both the cases, the model is loaded so that  $K_{Iq} = 2.32 \text{ MN/m}^{3/2}$ . For this value of  $K_{Iq}$ , the deformation profiles of the crack face when the load is applied at points A and B, respectively, are shown in Fig. 4. It is seen from Fig. 4 that for the same value of  $K_{Iq}$ : load (and displacements) at points A and B, respectively, are: 970.7N (and 0.615 mm) and 972.8N (and .74 mm). Thus when the load is modelled to act at B (the so-called "simplified loading case") there is more apparent input of energy to the specimen than when the load is modeled to act at A.

(the so-called "actual loading case") when an identical crack-length history as in Fig. 3 is used, but with the "actual loading condition", the computed dynamic k-factors are shown in Fig. 5. Comparing Figs. 2 and 5, it is seen that an apparently small modification in the load-condition modeling contributes to a substantial difference in the k-factor variation. It is seen that the results in Fig. 5, for the "actual loading case" agree remarkably well with the experimental results (considering the possible rate-sensitive behaviour of Araldite B as opposed to the present linear elastic modeling), and the peak in the present K-results is much smaller than that in Kobayashis' [8] results. The variation in energies W, U, T, F for the "actual loading case" is shown in Fig. 6. Comparing Fig. 3 and 6 it is seen that W in the "simplified loading case" is higher than in the "actual"; T is higher in the "simplified" than in the "actual", and that the variations of U and F are qualitatively similar in both the "loading cases".

The effect of the two loading cases for the RDCB specimen 17 is exhibited in Fig. 7. It is seen that for the same value of  $K_{Iq} = 1.33 \text{ MN/m}^{3/2}$ , the load (and displacement) at points A and B are, respectively: 556.5N (and 0.35 mm) and 557.7N (0.425 mm). Thus, once again, the apparent input energy to the specimen is larger in the "simplified loading case" than in the "actual loading case". This anomaly in modeling will have consequences in the "propagation" or "application" phase calculations in the RDCB No. 17 specimen to be discussed later.

#### "PROPAGATION" (OR "APPLICATION") CALCULATIONS

We now present calculations aimed at predicting crack-propagation history, and possible arrest, given the initial loading conditions and using the hypothesis that there is a given material toughness data in the form of a dynamic fracture-toughness-versus-crack-velocity-relation. Experimentally

evidence [6,7] that there is the possibility of a slight geometry dependence of this toughness property. The material toughness data surmised from the experimental findings of [6,7] for RDCB specimens, and tapered double cantilever beam specimens (TDCB) are shown in Fig. 8. In the present calculations, the RDCB and TDCB toughness data are used in the prediction of crack-propagation histories in RDCB and TDCB specimens, respectively. Calculations based on using RDCB toughness data for analysing TDCB specimens, and vice versa, are not reported here.

The results of the "propagation" or "application" type calculations for RDCB specimen 4, using the toughness property data of Fig. 8 and "simplified" boundary conditions, under plane stress conditions, are shown in Fig. 9. It is seen that the present predicted crack length at arrest is larger than in the experiment, even though the stress-intensity factor variation correlates well with the experimental result for most of the crack-propagation history. The respective results with the "actual boundary conditions", and under plane stress conditions, are shown in Fig. 10. It can be seen from Fig. 10 that the presently calculated length history, crack-velocity history, as well as the K-factor variation, are all in remarkably good agreement with the experimental results. It is noted that the present peak value in the K-factor is much closer to the experimental result, than that in the solution by Kobayashi [8]. To compare the effects of plane stress versus plane strain conditions, a "propagation" calculation was performed on the RDCB No. 4. Specimen, with "simplified boundary conditions", and the results are shown in Fig. 11. Comparing Fig. 9 and 11, it is seen noticeable difference can be found between the stress-intensity factor variation between the two cases in the initial phase of the crack propagation history, and the final crack-arrest length is much higher in the plane stress case than in the plane-strain case.

The energy variations,  $U$ ,  $T$ ,  $F$  and  $W$  for the cases: (i) plane-stress, simplified loading case, (ii) plane-stress, "actual loading case", and (iii) plane-strain, simplified loading case, are shown in Figs. 12, 13, and 14 respectively. Comparing Fig. 12 and 13 it is seen that the ratio of maximum kinetic energy to input energy in the simplified loading case (0.278) is much larger than in the actual loading case (0.233), while the crack arrest length, comparing Figs. 9, and 10, is much larger in the "simplified loading case" than in the "actual loading" case. Likewise, comparing Figs. 12 and 14, it is seen that the ratio of maximum kinetic energy to input energy in the plane-strain case (0.266) is smaller than in the plane-stress case (0.278), while the crack arrest length is smaller in the plane strain case as compared to the plane-stress case.

The crack-surface deformation profile for the propagating crack in RDCB No. 4 specimen are shown in Fig. 15 for various instances of time. Noting the essentially linear shapes of these profiles, except asymptotically close to the crack-tip, the possibility exists to devise simple method to find the stress-intensity factors from the crack-mouth opening displacement. This possibility is successfully explored in [11]. Figs. 16 through 21 show the contours of principal-stress difference values at various instances of time in the moving-singularity element of the RDCB 4 specimen model, in the plane stress case. The sequential pictures demonstrate graphically, not only the singular-stress-field but the total stress field, and its magnification near the propagating crack-tip. Since in the present finite element method, the effects of stress-wave interactions are accurately accounted for, and the total stress (singular as well as nonsingular) field can be computed accurately, results similar to these as well as the results for circumferential stress  $\sigma_{00}$  (not shown here) can be used in the analysis of crack-branching. Such studies will be presented else-

where, shortly.

The results for RDCB 17 specimen for: (i) plane stress, simplified loading case, and (ii) plane stress, actual loading case, are shown in Figs. 22 and 23 respectively. Comparing Figs. 22 and 23, it is seen that the higher crack arrest length in the simplified loading case than in the actual loading case can be attributed to the higher apparent input energy in the former than in the latter case, as seen from Fig. 7. In the plane-stress, actual loading case, the calculation was continued for a sufficient time after crack arrest ( $t \geq 320$  sec), and the observed oscillation in K-factor is shown in Fig. 24. This oscillation is qualitatively similar to that recorded in the experiments [6]. The results for the plane-strain, simplified loading case, are shown in Fig. 25. In comparing Figs. 22 and 25, comments essentially similar to those made in comparing Figs. 9 and 11, can be made. The energy variations in RDCB 17 specimen for: (i) plane-stress, simplified loading case; (ii) plane-stress actual loading case, and (iii) plane-strain, simplified loading case, are shown in Figs. 26, 27, and 28, respectively. Again, in comparing Figs. 26, 27, and 28, comments essentially similar to those in connection with the comparison of Figs. 12, 13, and 14, respectively, can be made. Thus there is a correlation between the ratio of the maximum kinetic energy to input energy, and the crack arrest length. The crack-surface deformation profiles at various instants of time in RDCB 17 specimen shown in Fig. 29 are similar to those in Fig. 15 for specimen 4. Results such as in Figs. 15 and 29 form the basis for methods of obtaining K from crack-mouth-opening displacements discussed by the authors elsewhere [11].

The finite element model for the tapered double cantilever beam (TDCB) specimen is shown in Fig. 30. The cross-hatched element shown in Fig. 30 is the authors' moving singularity element, and the mesh shown in Fig. 30 is thus at the beginning of crack propagation.

As in RDCB specimen, two loading cases were considered: (i) the edge loading case wherein load is supposed to act at point B, and (ii) the actual pin loading case wherein the load is modeled to act at point A in Fig. 30. Plane stress conditions are invoked in both the loading cases. The influence of loading position is demonstrated in Fig. 31. In all the cases shown in Fig. 31, the model is loaded so that  $K_{Iq} = 2.08 \text{ MN/m}^{3/2}$ . As the loading point approaches to the specimen surface while keeping the  $x_1$ -coordinate constant, the displacement at the loading point becomes larger while the reaction force is almost constant, thus the input energy to the specimen becomes higher. The input energy in the edge loading (loading point B) is also shown in Fig. 31. It is seen that the input energy in the edge loading case is much higher than that in the actual loading case.

The computed results for  $K_{\Sigma}(t)$ ,  $\Sigma(t)$  and  $\dot{\Sigma}(t)$  for both the loading cases are shown in Figs. 32 and 33 respectively. In the edge loading case as shown in Fig. 32, after 240  $\mu\text{sec}$  the stress intensity factor becomes almost constant and the crack propagation with a relatively slow speed ( $v \approx 100 \text{ m/sec}$ ). In the actual loading case, however, as shown in Fig. 33 the crack was arrested earlier than in the edge loading case. The  $K_x$  value variation with crack length for the actual as well as edge loading case is shown in Fig. 34. The result in the actual loading case shows better agreement with the experimental results obtained by Kalthoff et al [7].

The energy variations for the edge loading and actual loading cases are shown in Fig. 35 and 36 respectively. Comparing Figs. 35 and 36 it is seen that the ratio of maximum kinetic energy to input energy in the edge loading case (0.132) is much larger than that in the actual loading case (0.093). As also observed in the RDCB specimen, the ratio of maximum kinetic energy to input energy correlates with the crack arrest length, i.e., increasing  $\Sigma_{\text{arr}}$  with

the increasing value of  $(\max T/W)$ . Here the correlation between the total energy  $(U+T+F)$  and the input energy  $W$  in the TDCB specimen is much better than in the RDCB specimen as shown earlier.

The crack opening profiles in the edge loading case, at various instants of time, are shown in Fig. 37. Because of the loading at the edge of the specimen, these profiles are distinctly nonlinear as compared to those in actual loading case (see Figs. 15 and 29 in the RDCB specimen).

Finally, Figs. 38 to 42 exhibit sequentially, the contours of principal-stress difference at various instants of time in the moving-singularity element of the TDCB specimen with the edge loading. It is noted that the size of the moving-singularity element (16x8) mm for the TDCB specimen while it is (42x21) mm for the RDCB specimen. Comparing Figs. 16 to 21 on the one hand, and Figs. 38 to 42 on the other, it is seen that the effects of crack-propagation and stress wave interactions are more complex in the TDCB specimen than in the RDCB specimen.

#### Concluding Remarks:

The results presented above indicate that the presently developed computational procedures are capable of accurately predicting dynamic crack propagation and arrest, based on the hypothesis that there exist a "reasonable" geometry independent material property in the form of a dynamic-fracture-toughness-versus-crack velocity. The results also demonstrate the importance of modeling the loading conditions and other boundary conditions highly accurately, in an elastodynamic crack propagation problem.

However, other questions that may be germane to the subject of dynamic fracture mechanics itself, such as the load-rate sensitivity of dynamic fracture toughness, etc., need to be resolved before the power of the present procedures can be fully tested. These questions, while not forming the subject of the present paper, have been attempted to be discussed by the authors [12], and others [10] elsewhere.

Acknowledgements:

This work was supported by ONR under Contract 78-C-0036, and by AFOSR under Grant 81-0057. The authors are grateful for this support. They express their sincere appreciation to Ms. Margarete Eiteman for her careful assistance in preparing this manuscript.

References:

- [1] Kanninen, M.F., "A Critical Appraisal of Solution Techniques in Dynamic Fracture Mechanics", in Numerical Methods in Fracture Mechanics, (A.R. Luxmore & D.R.J. Owen, Eds.), Pineridge Press, Swansea, U.K., 1978, pp. 612-634.
- [2] Atluri, S.N., Nishioka, T., and Nakagaki, M., "Numerical Modeling of Dynamic & Nonlinear Crack Propagation in Finite Bodies, By Moving Singular Elements", in Nonlinear and Dynamic Fracture Mechanics, (N. Perrone & S.N. Atluri, Eds.) ASME AMD Vol. 35, 1979, pp. 37-67.
- [3] Nishioka, T., and Atluri, S.N., "Numerical Modeling of Dynamic Crack Propagation in Finite Bodies, by Moving Singular Elements: Part I - Formulation", ASME Journal of Applied Mechanics, Vol. 47, No. 3, 1980, pp. 570-576.
- [4] Nishioka, T., and Atluri, S.N., "Numerical Modeling of Dynamic Crack Propagation in Finite Bodies, by Moving Singular Elements: Part II - Results", ASME Journal of Applied Mechanics, Vol. 47, No. 3, 1980, pp 577-583.
- [5] Nishioka, T., Stonesifer, R.B., and Atluri, S.N., "An Evaluation of Several Moving Singularity Finite Element Models for Fast Fracture Analysis", Engineering Fracture Mechanics, 1981, (In Press).
- [6] Kalthoff, J.F., Beinert, J., and Winkler, S., "Measurements of Dynamic Stress Intensity Factors for Fast Running and Arresting Cracks in Double-Cantilever-Beam Specimens", Fast Fracture and Crack Arrest, ASTM STP 627 (G.T. Hahn et al, Eds.), 1977, pp. 161-176.
- [7] Kalthoff, J.F., Beinert, J., and Winkler, S., "Influence of Dynamic Effect on Crack Arrest", Institut für Festkörpermechanik, EPRI Contract Report, RP-1022-1, 1978, IKFM40412.
- [8] Kobayashi, A.S., "Dynamic Fracture Analysis By Dynamic Finite Element Method-Generation and Propagation Analyses" in Nonlinear & Dynamic Fracture Mechanics, (N. Perrone & S.N. Atluri, Eds.), ASME, AMD Vol. 35, 1979, pp. 19-37.
- [9] Popelar, C.H., and Gehlen, P.C., "Modeling of Dynamic Crack Propagation: II Validation of Two-Dimensional Analysis", Int. Jnl. of Fracture Vol. 15, 1979, pp. 159-178.

- [10] Kanninen, M.F., Gehlen, P.C., Barnes, R.C., Hoagland, R.G., Hahn, G.T. and Popelar, C.H., "Dynamic Crack Propagation Under Impact Loading", in Nonlinear & Dynamic Fracture Mechanics, (N. Perrone, & S.N. Atluri, Eds.) ASME AMD Vol. 35, 1979, pp. 195-201.
- [11] Nishioka, T., and Atluri, "A Method for Determining Dynamic Stress Intensity Factors from COD Measurement at the Notch Mouth in Dynamic Tear Testing", Engineering Fracture Mechanics (to appear).
- [12] Nishioka, T., Perl, M., and Atluri, S.N., "An Analysis of, and Some Observations on, Dynamic Fracture in an Impact Test Specimen", ASME, Pressure Vessels and Piping Conference, June 21-25, 1981, Denver, CO, Preprint No. 81-PVP-18.

Figure Captions:

Fig. 1: Finite element model for RDCB specimen

Fig. 2: Variation of dynamic stress intensity factors in RDCB No. 4 with simplified loading (generation phase)

Fig. 3: Energy variations in RDCB No. 4 with simplified loading (generation phase)

Fig. 4: Crack opening profiles in RDCB No. 4 with different loading conditions

Fig. 5: Variation of dynamic stress intensity factors in RDCB No. 4 with actual loading (generation phase)

Fig. 6: Energy variation in RDCB No. 4 with actual loading (generation phase)

Fig. 7: Crack opening profiles in RDCB No. 17 with different loading conditions

Fig. 8: Crack velocity versus dynamic fracture toughness relations for Araldite B epoxy (Kalthoff et al)

Fig. 9: Variation of dynamic stress intensity factors in RDCB No. 4 with simplified loading (application phase, plane stress)

Fig. 10: Variation of Dynamic stress intensity factors in RDCB No. 4 with actual loading (application phase, plane stress)

Fig. 11: Variation of dynamic stress intensity factors in RDCB No. 4 with simplified loading (application phase, plane strain)

Fig. 12: Energy variations in RDCB No. 4 with simplified loading (application phase, plane stress)

Fig. 13: Energy variations in RDCB No. 4 with actual loading (application phase, plane stress)

Fig. 14: Energy variations in RDCB No. 4 with simplified loading (application phase, plane strain)

Fig. 15: Variation of crack opening profiles in RDCB No. 4 (actual loading)

Fig. 16: Contours of principal-stress difference in RDCB No. 4 ( $t=0.0\mu\text{sec}$ )

Fig. 17: Contours of principal-stress difference in RDCB No. 4 ( $t=100\mu\text{sec}$ )

Fig. 18: Contours of principal-stress difference in RDCB No. 4 ( $t=200\mu\text{sec}$ )

Fig. 19: Contours of principal-stress difference in RDCB No. 4 ( $t=300\mu\text{sec}$ )

Fig. 20: Contours of principal-stress difference in RDCB No. 4 ( $t=400\mu\text{sec}$ )

Fig. 21: Contours of principal-stress difference in RDCB No. 4 ( $t=528\mu\text{sec}$ )

Fig. 22: Variation of dynamic stress intensity factors in RDCB No. 17 with simplified loading (plane stress)

Fig. 23: Variation of dynamic intensity factors in RDCB No. 17 with actual loading (plane stress)

Fig. 24: Variation of dynamic stress intensity factors in RDCB No. 17 after crack arrest

Fig. 25: Variation of dynamic stress intensity factors in RDCB No. 17 with simplified loading (plane strain)

Fig. 26: Energy variation in RDCB No. 17 with simplified loading (plane stress)

Fig. 27: Energy variations in RDCB No. 17 with actual loading (plane stress)

Fig. 28: Energy variations in RDCB No. 17 with simplified loading (plane strain)

Fig. 29: Variation of crack opening profiles in RDCB No. 17 (actual loading)

Fig. 30: Finite element model for TDCB specimen

Fig. 31: Input energy variation in TDCB specimen with various loading points

Fig. 32: Variation of stress intensity factors in TDCB specimen with edge loading

Fig. 33: Variation of stress intensity factors in TDCB specimen with actual loading

Fig. 34: Dynamic stress intensity factor versus crack length relations for TDCB specimen

Fig. 35: Energy variations in TDCB specimen with edge loading

Fig. 36: Energy variations in TDCB specimen with actual loading

Fig. 37: Variation of crack opening profiles in TDCB specimen with edge loading

Fig. 38: Contours of principal-stress difference in TDCB specimen ( $t=0.0\mu\text{sec}$ )

Fig. 39: Contours of principal-stress difference in TDCB specimen ( $t=100\mu\text{sec}$ )

Fig. 40: Contours of principal-stress difference in TDCB specimen ( $t=200\mu\text{sec}$ )

Fig. 41: Contours of principal-stress difference in TDCB specimen ( $t=300\mu\text{sec}$ )

Fig. 42: Contours of principal-stress difference in TDCB specimen ( $t=400\mu\text{sec}$ )

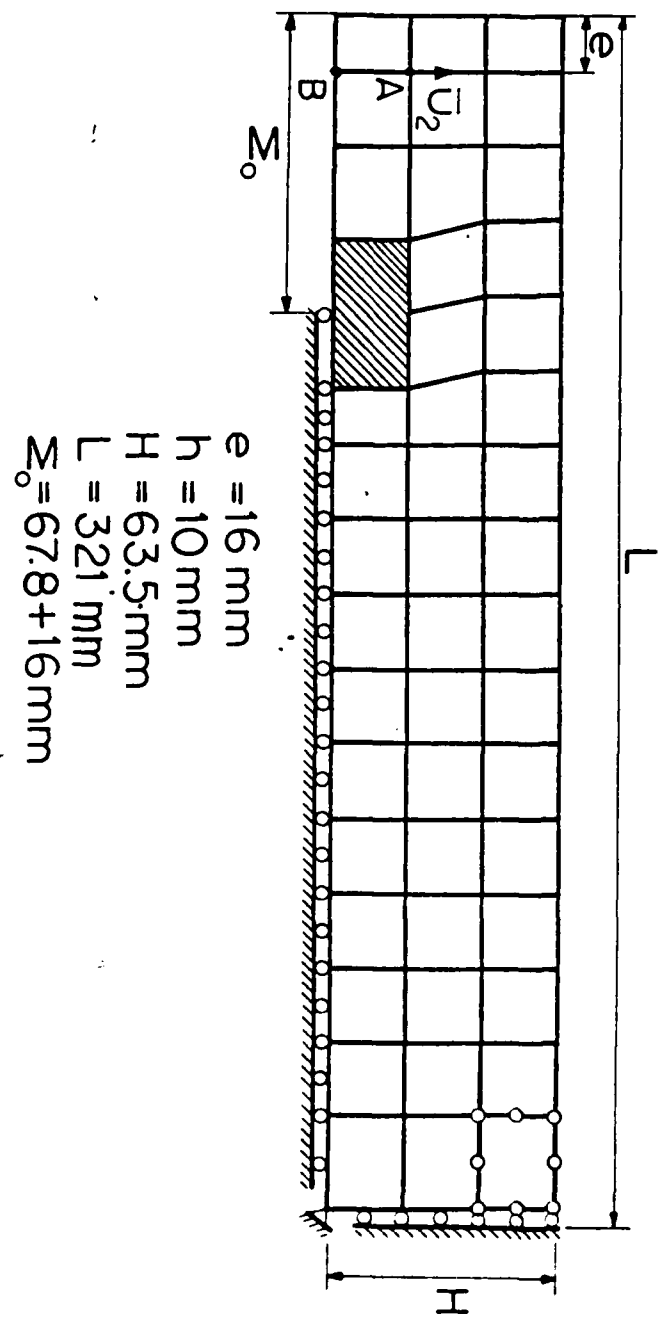
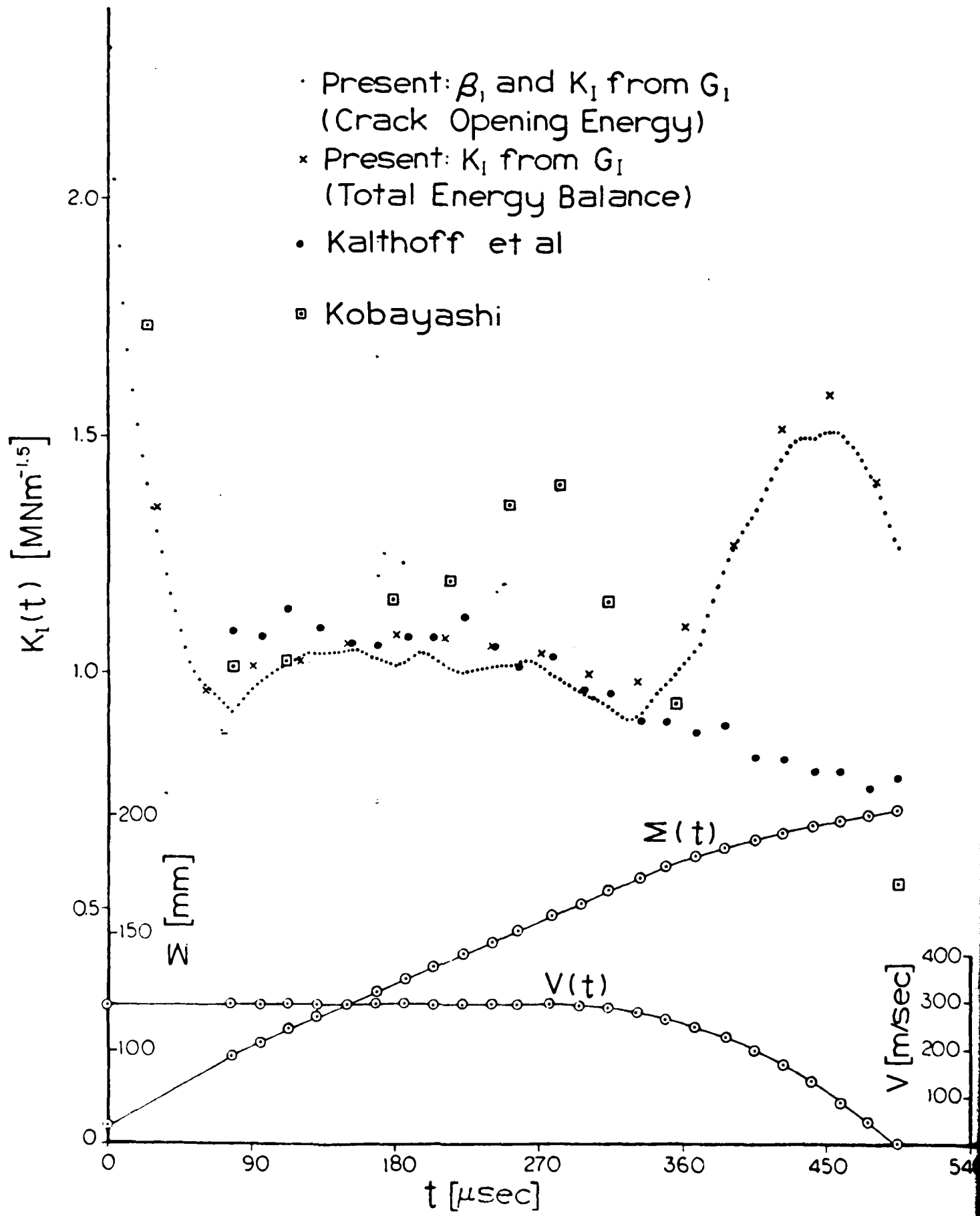


Fig. 1



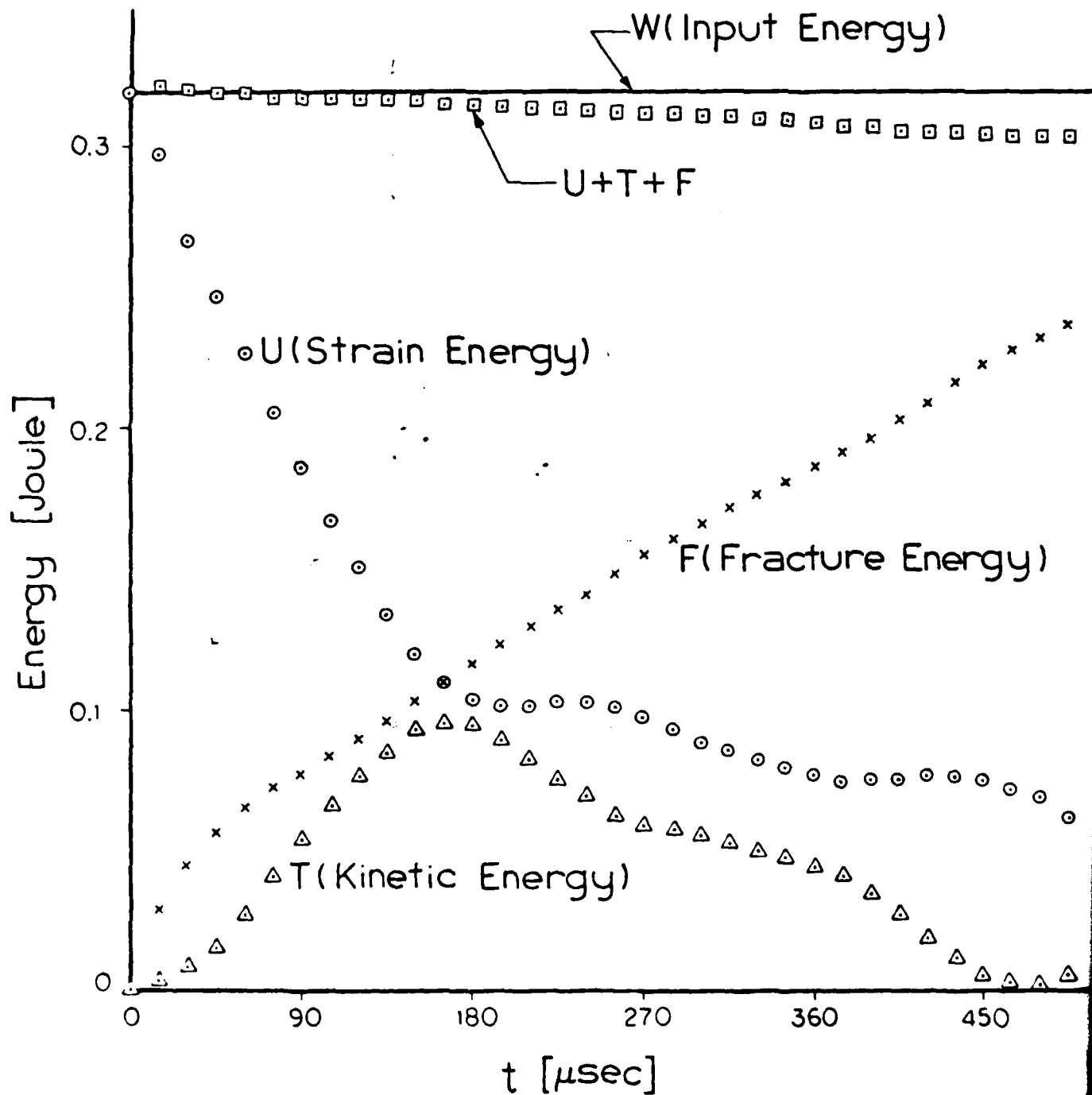


Fig. 3

RDCB No.4

○ A

△ B

Reaction force at A 970.7 N  
at B 972.8 N

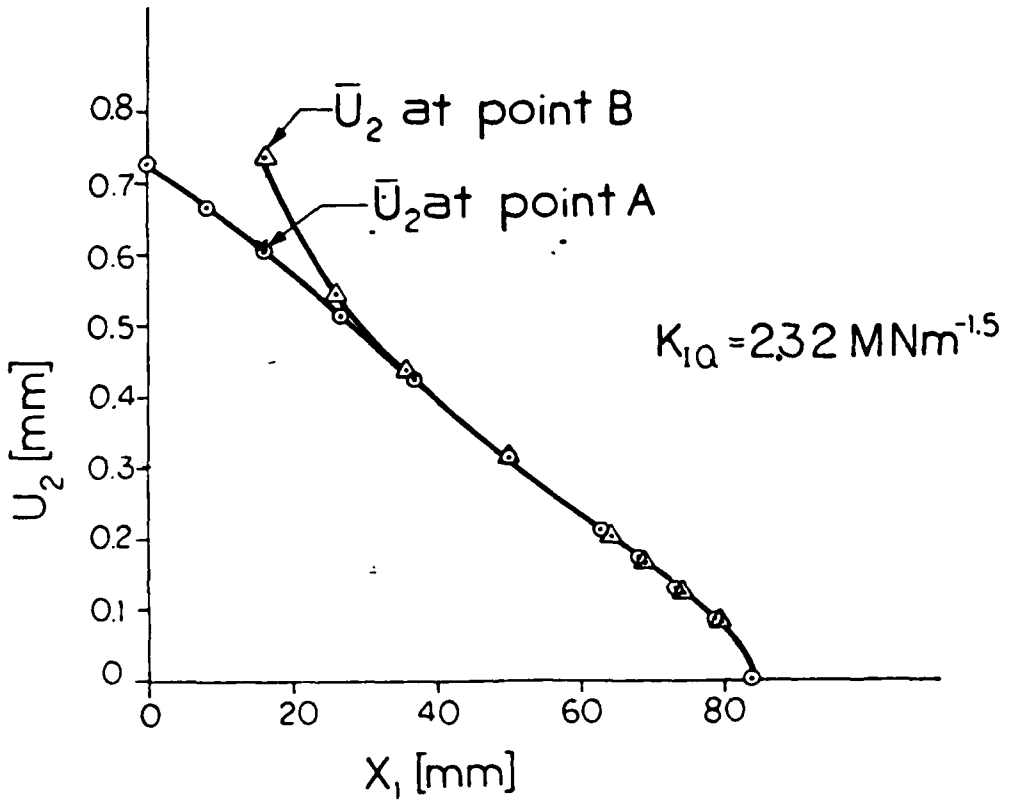
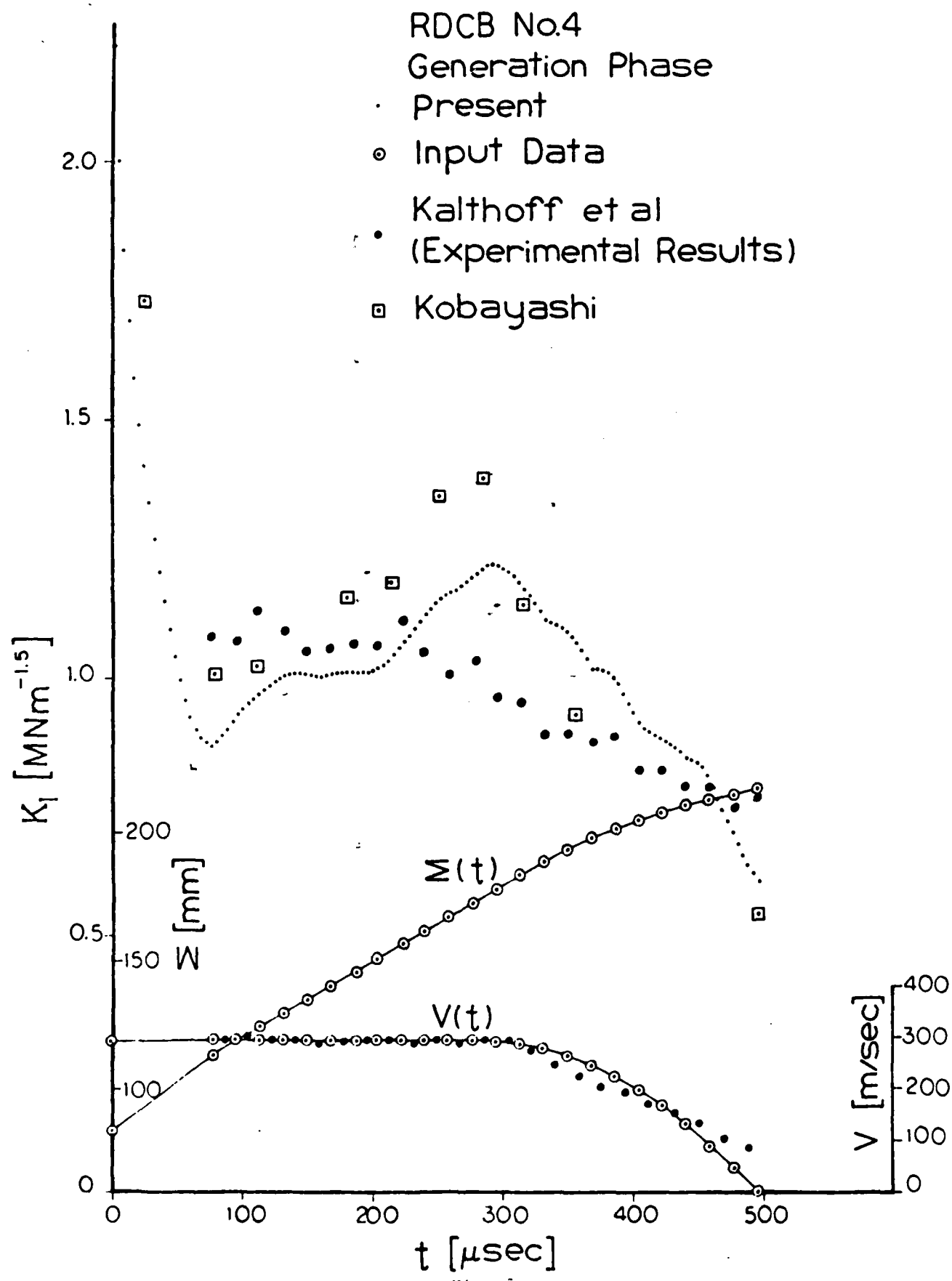
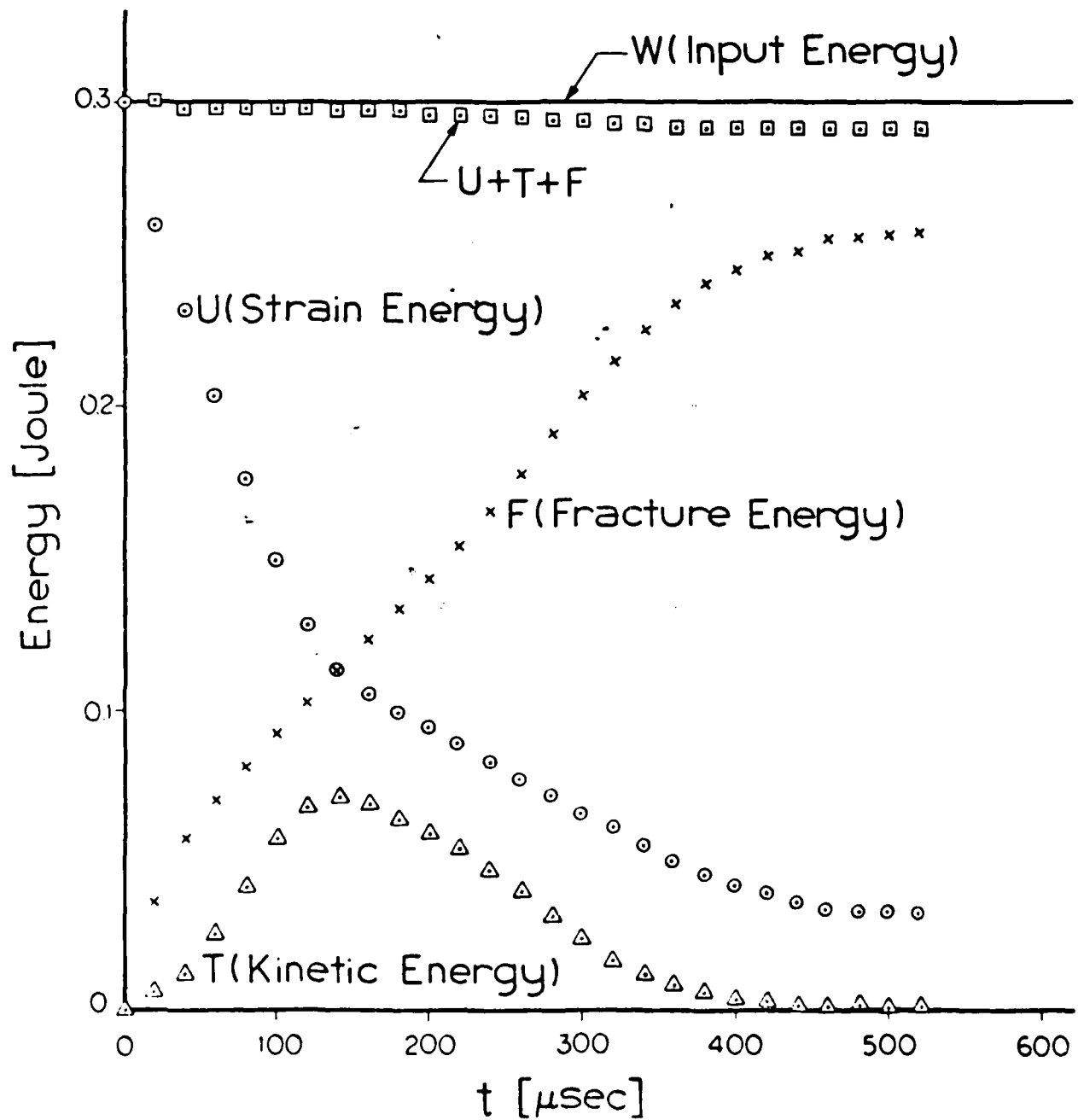


Fig. 4



RDCB No4 Specimen  
Plane Stress  
Application Phase



RDCB No.17

○ A

△ B

Reaction force at A 556.5 N  
at B 557.7 N

Crack opening displacement

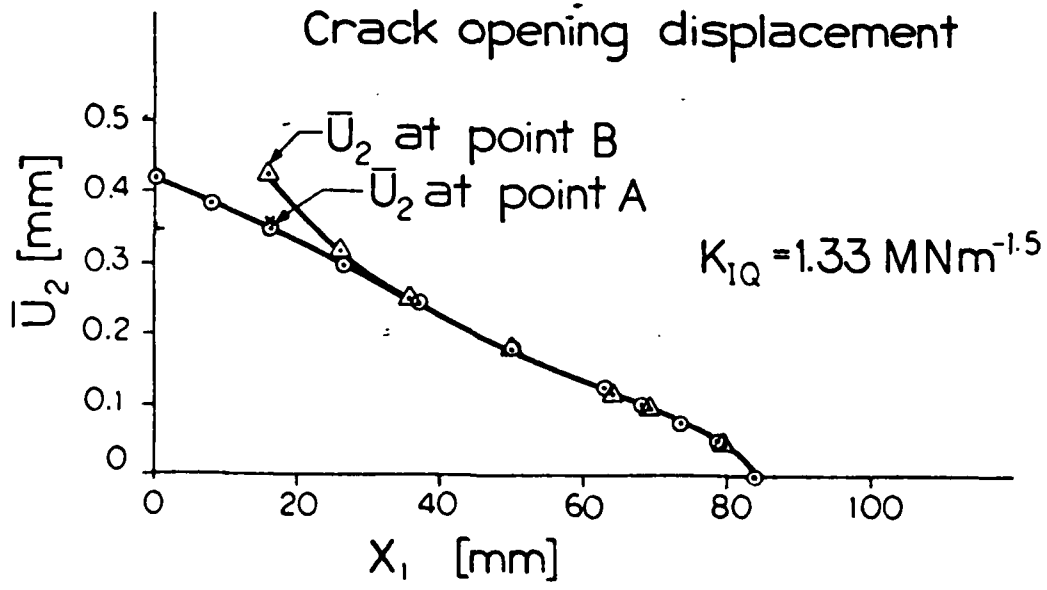


Fig. 7

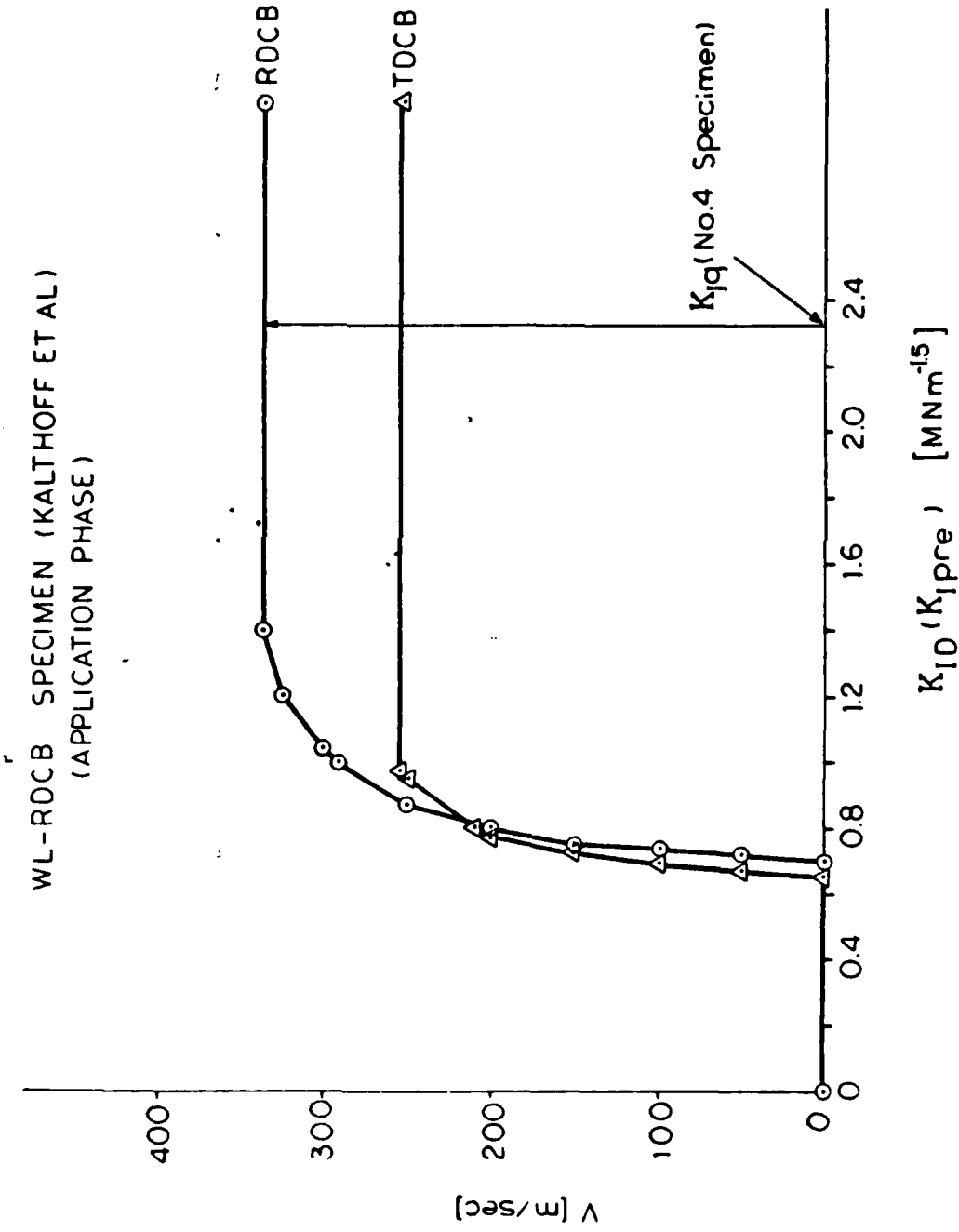


Fig. 8

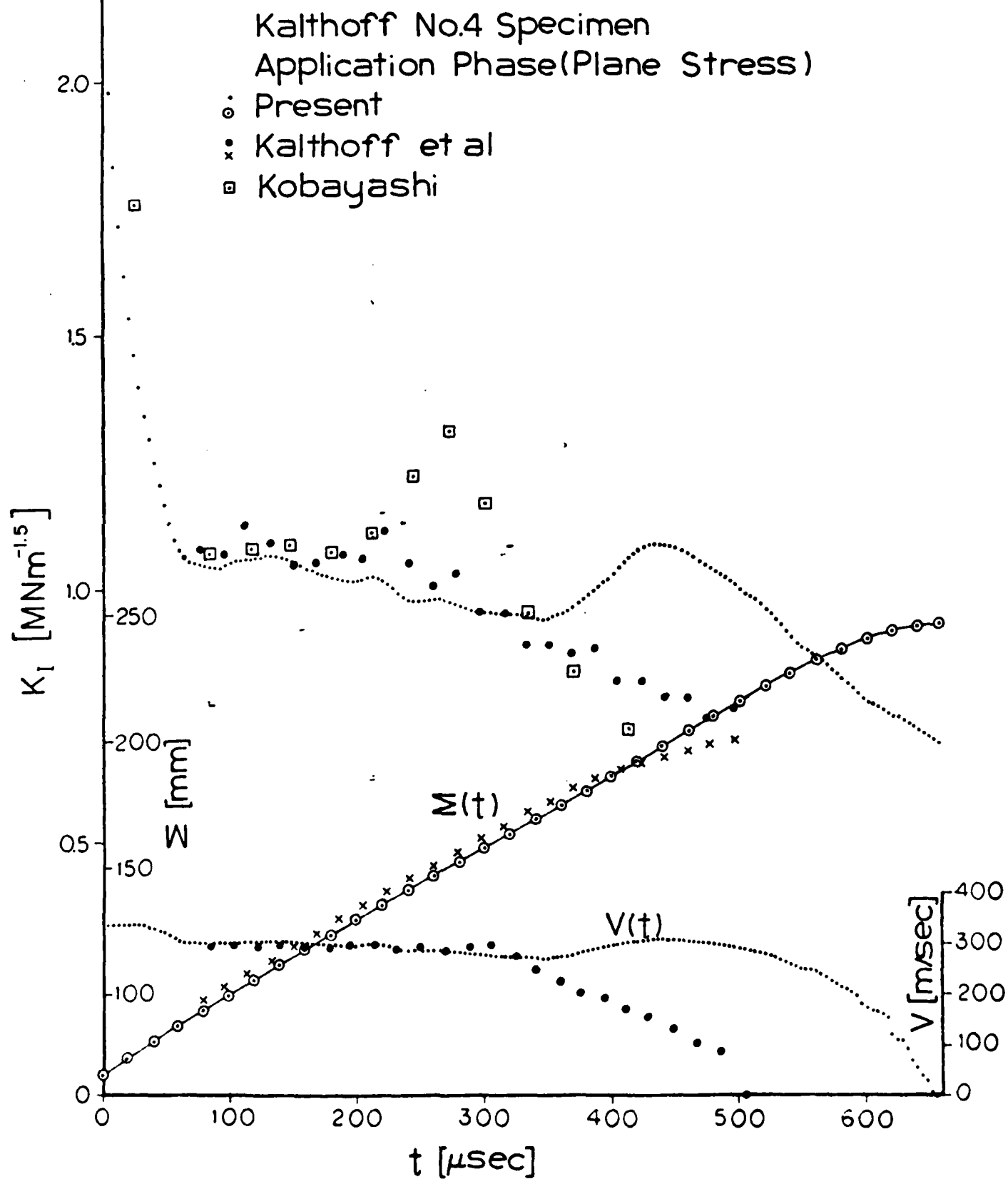


Fig. 9

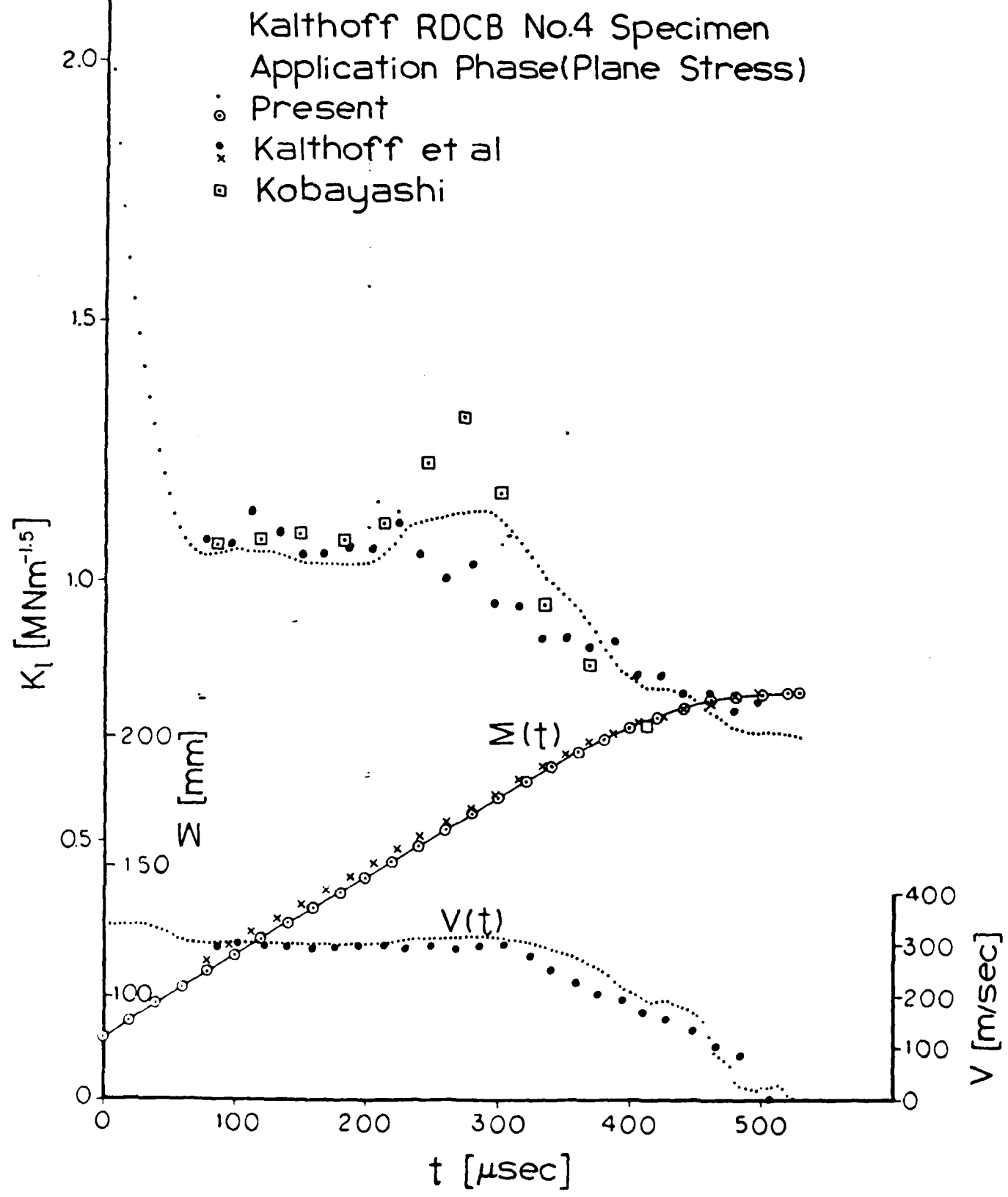
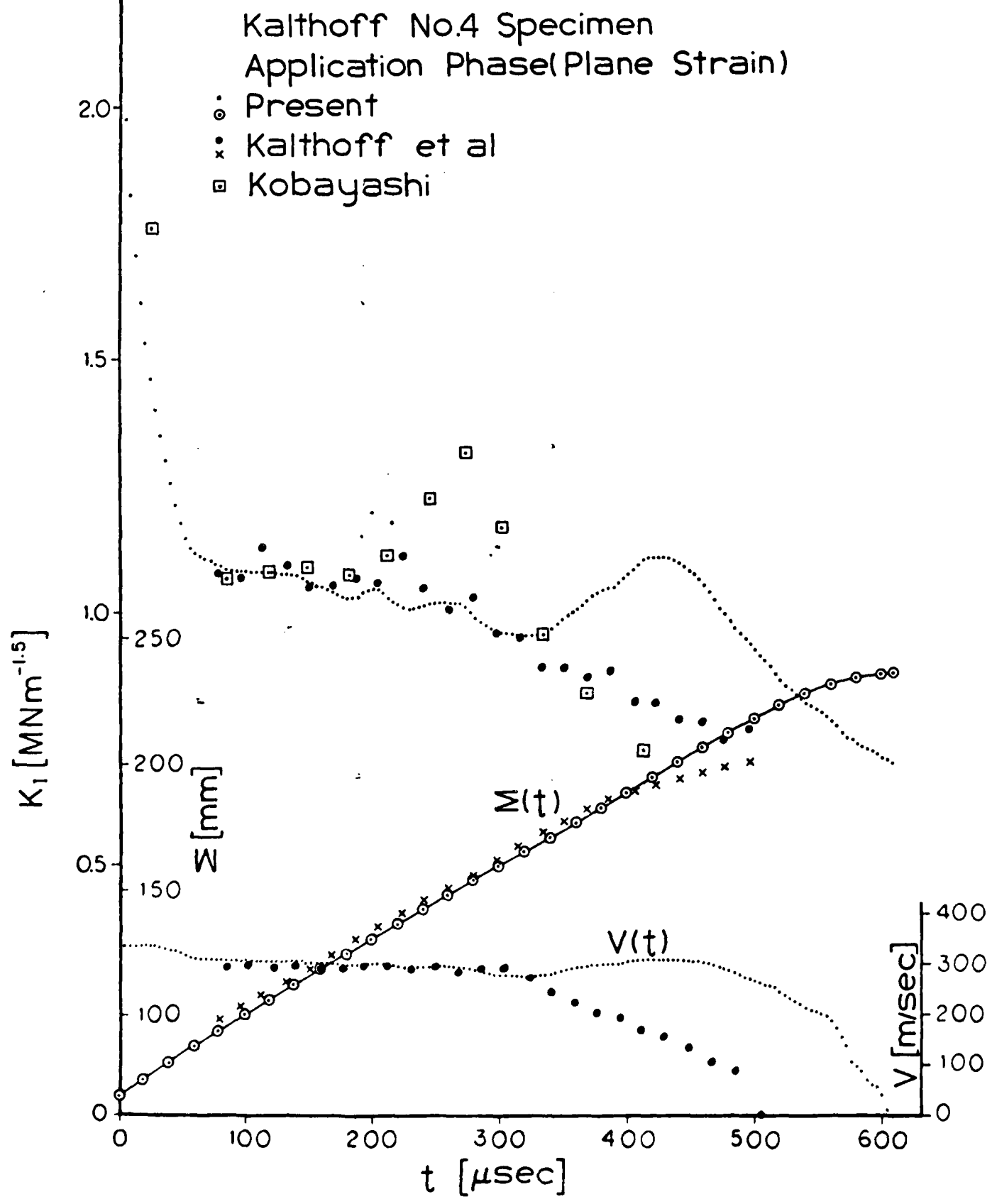


FIG. 10



Kalthoff No.4 Specimen  
Application Phase  
Plane Stress

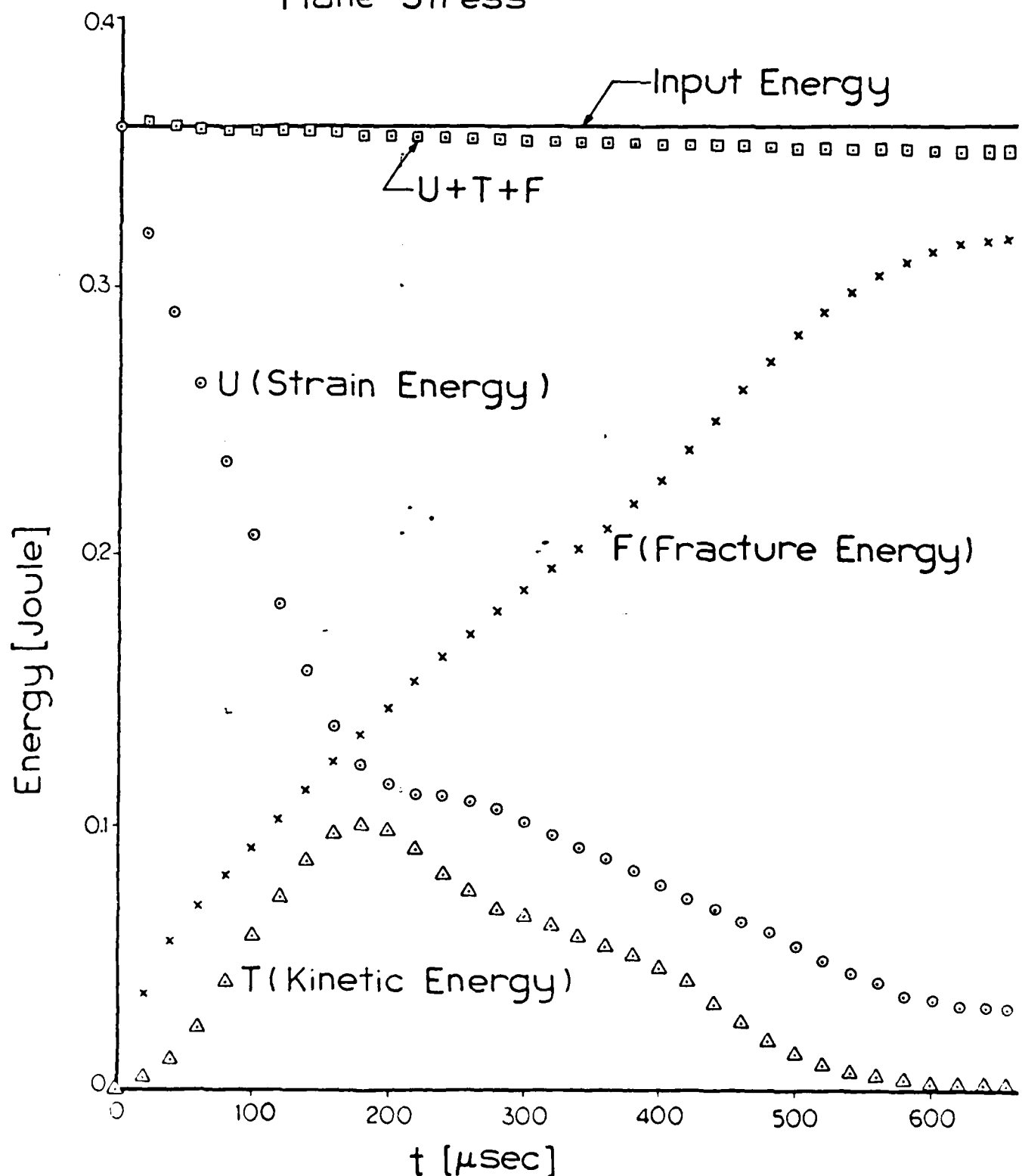


Fig. 12

RDCB No.4 Specimen  
Plane Stress  
Generation Phase

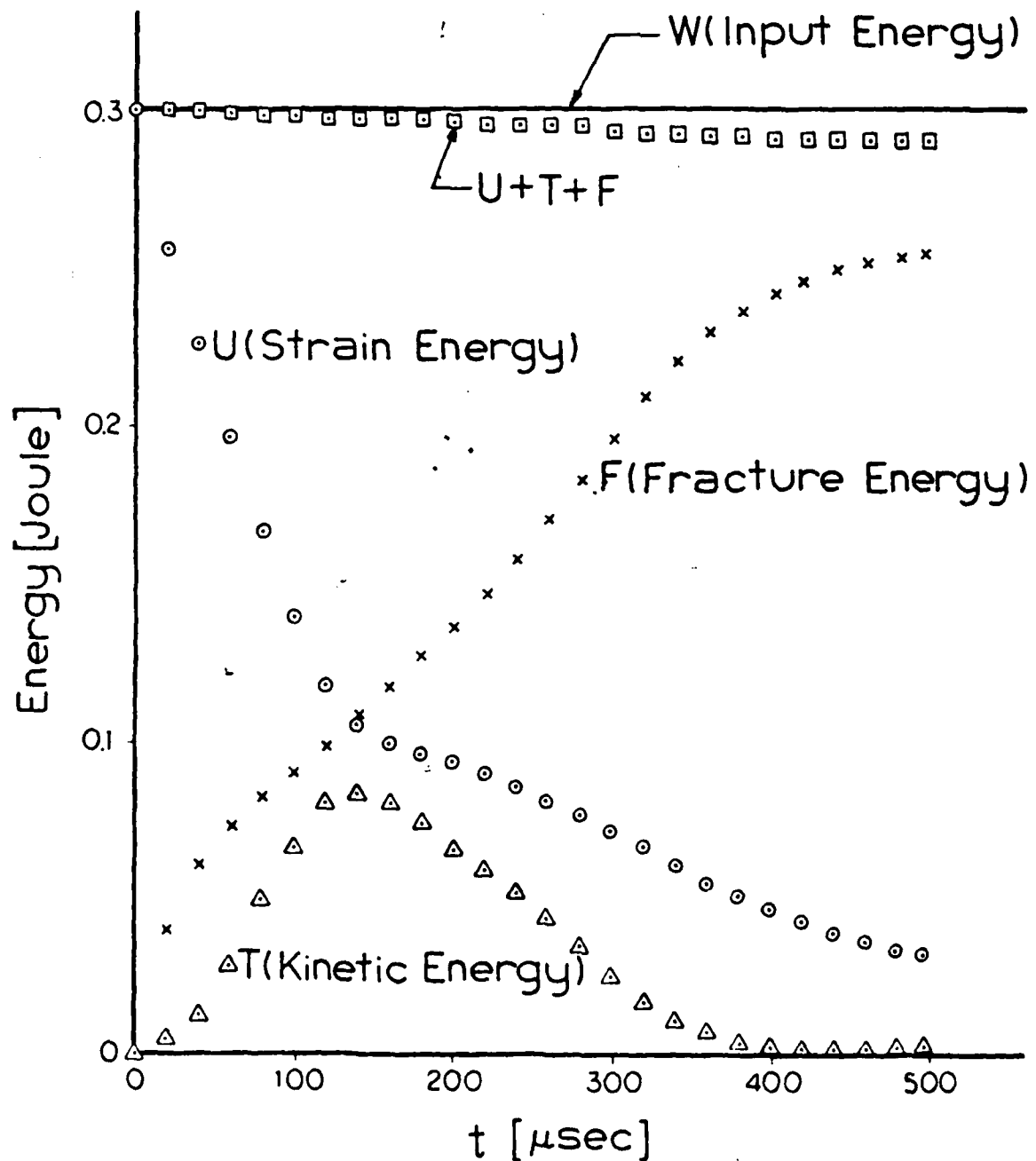


Fig. 13

Kalthoff No.4 Specimen  
Plane strain  
(Application phase)

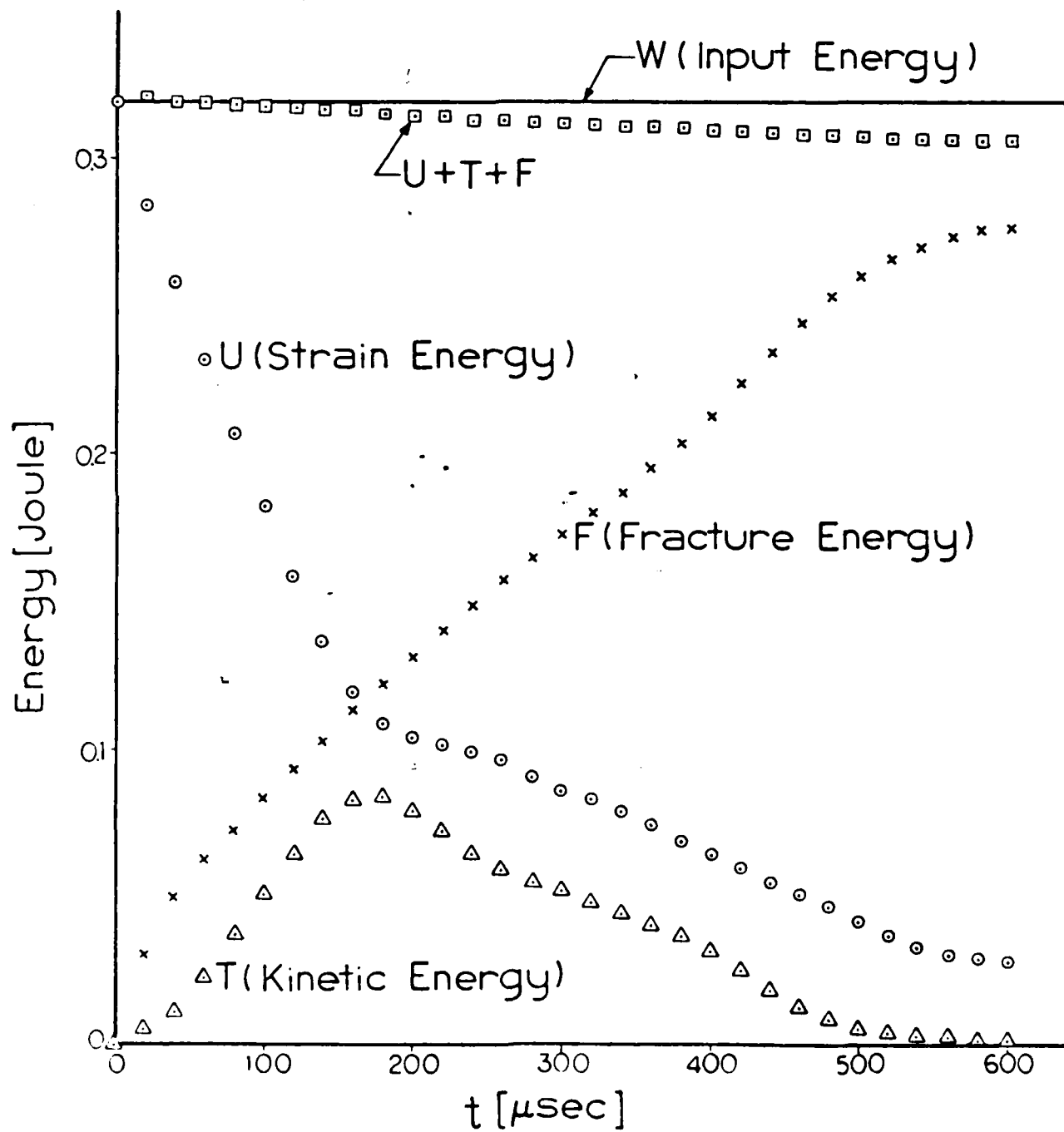


Fig. 14

RDCB No.4 Specimen  
Application Phase  
Plane Stress

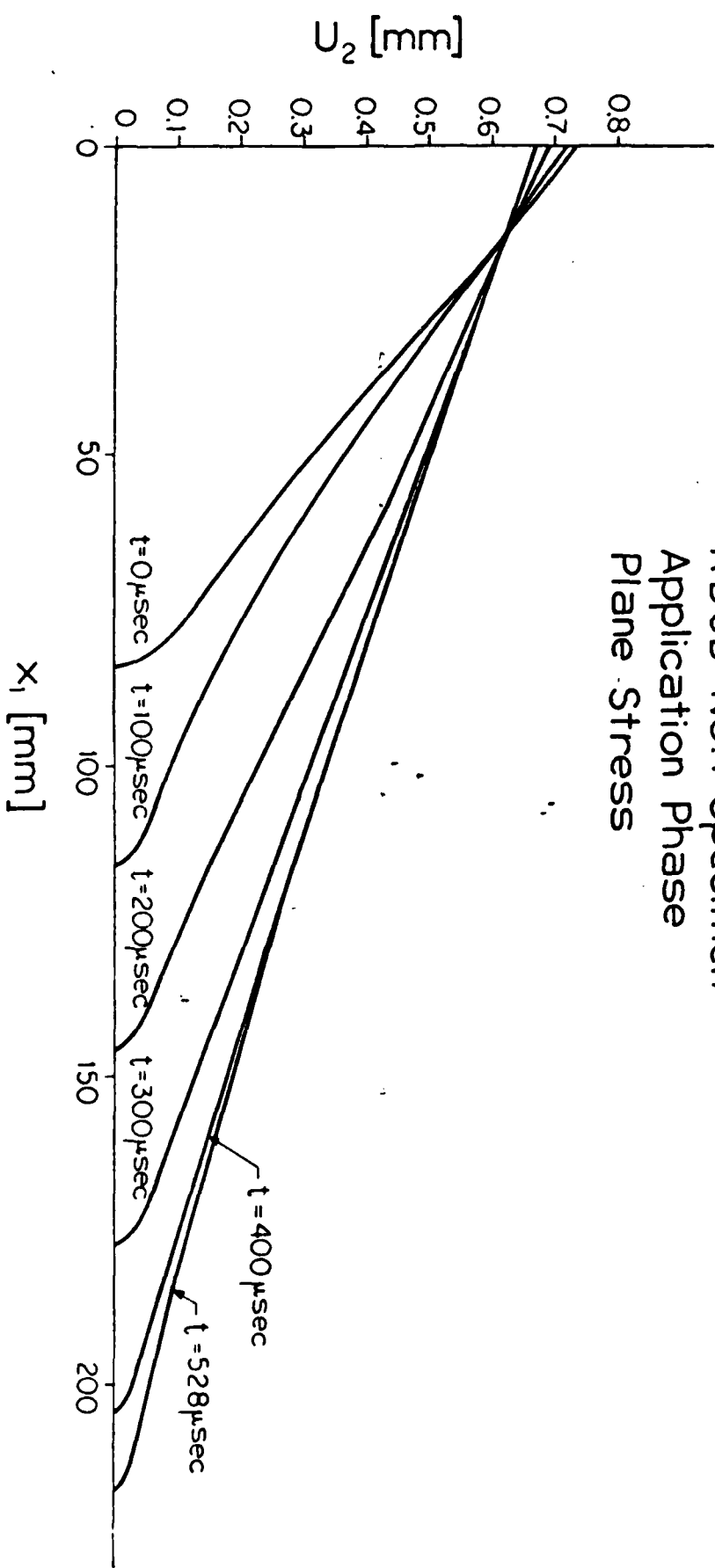


Fig. 15

# RDCB No.4 Specimen Application Phase Plane Stress

$$K_1 = 2.32 \text{ MNm}^{-1.5}$$

M  
=  
33.8  
m

卷之三

-001SEC

1 = U.U  $\mu$ SC C

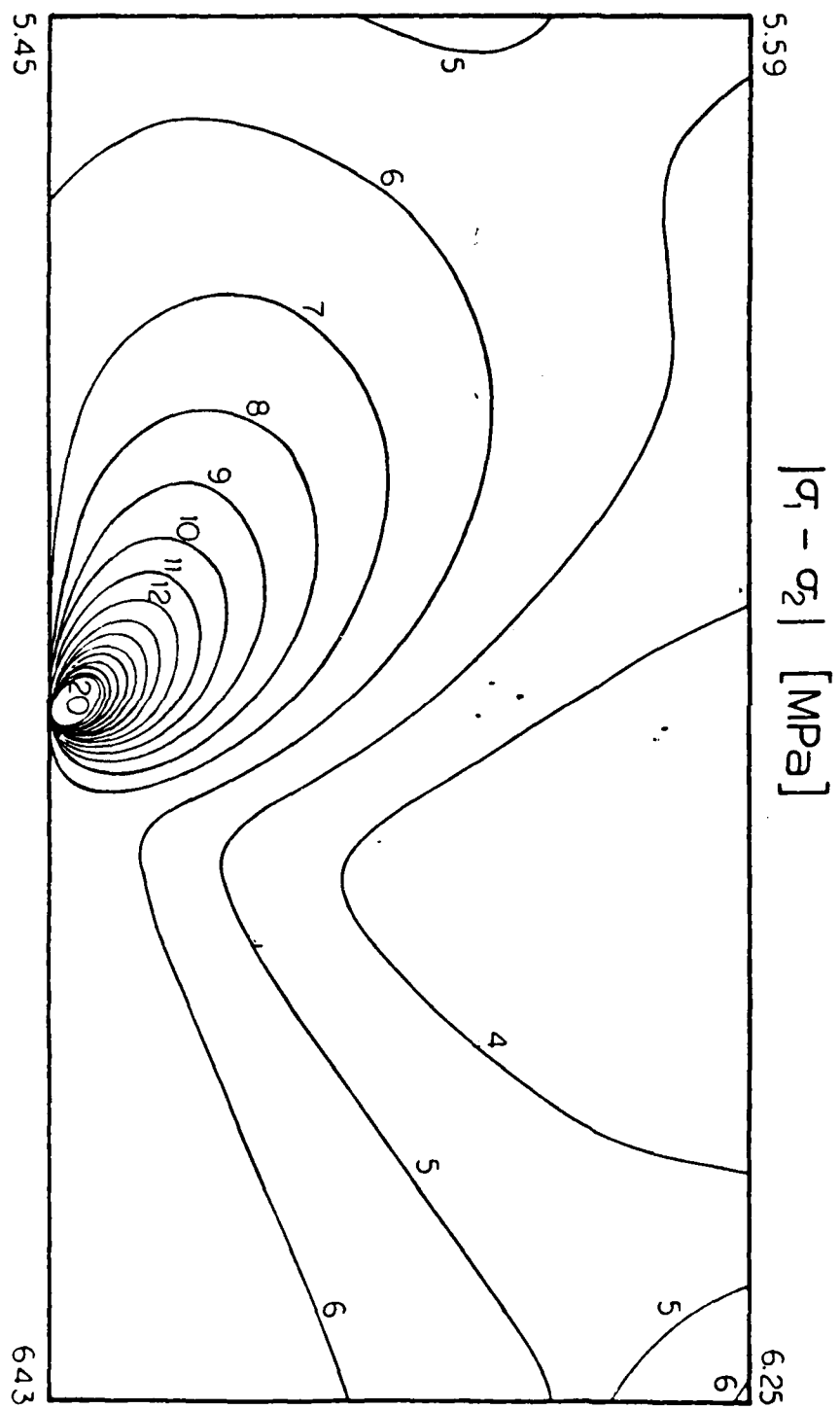


Fig. 16

RDGB No.4 Specimen       $K_I = 1.059 \text{ MNm}^{-1.5}$   
 Application Phase       $\Delta = 115.7 \text{ mm}$   
 Plane Stress       $V = 302.9 \text{ m/sec}$   
 t =  $100 \mu\text{sec}$

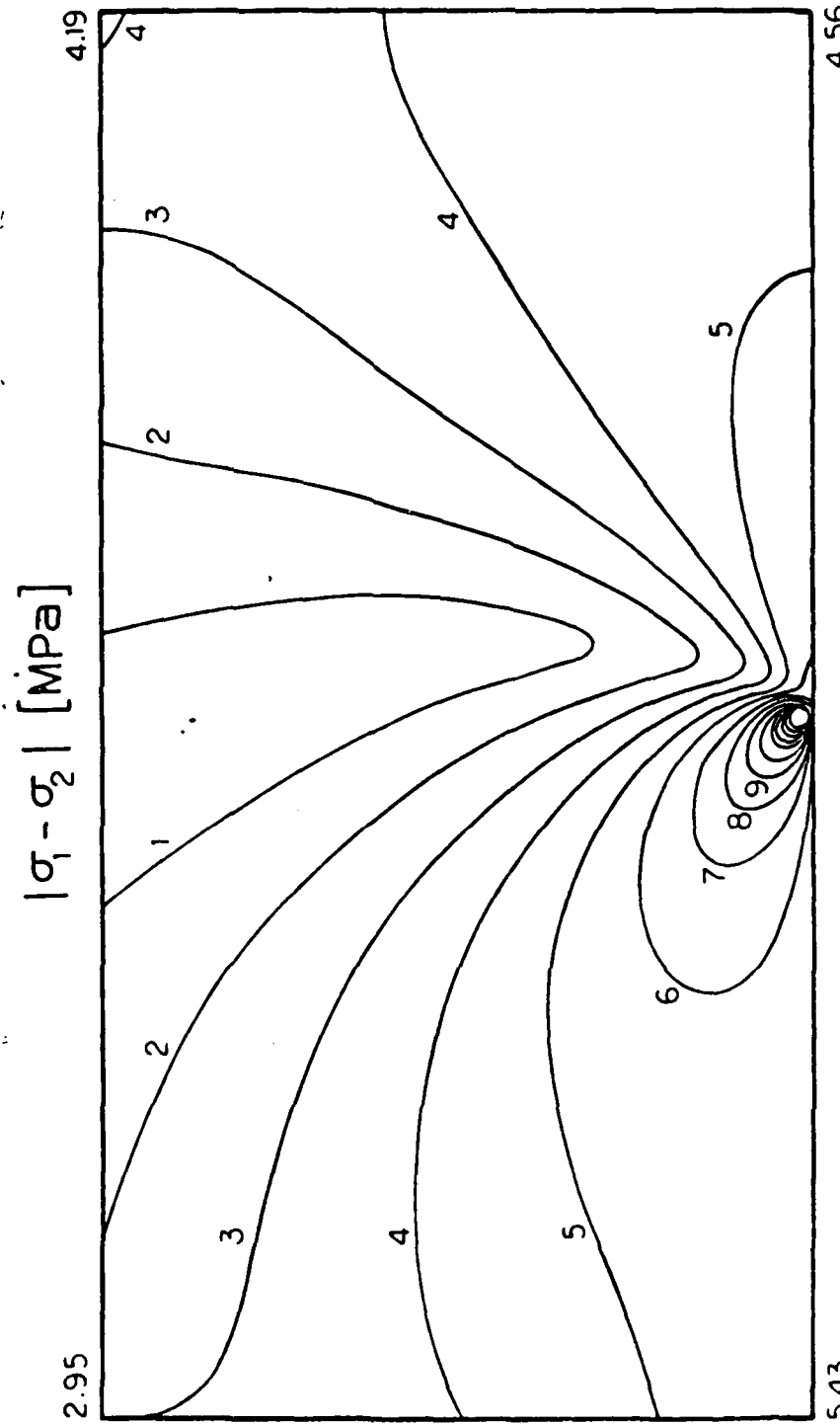


Fig. 17

RDCB No.4 Specimen  
Application Phase  
Plane Stress

$K_I = 1.034 \text{ MNm}^{-1/2}$   
 $\Sigma = 145.6 \text{ mm}$   
 $V = 298.3 \text{ m/sec}$   
 $t = 200 \mu\text{sec}$

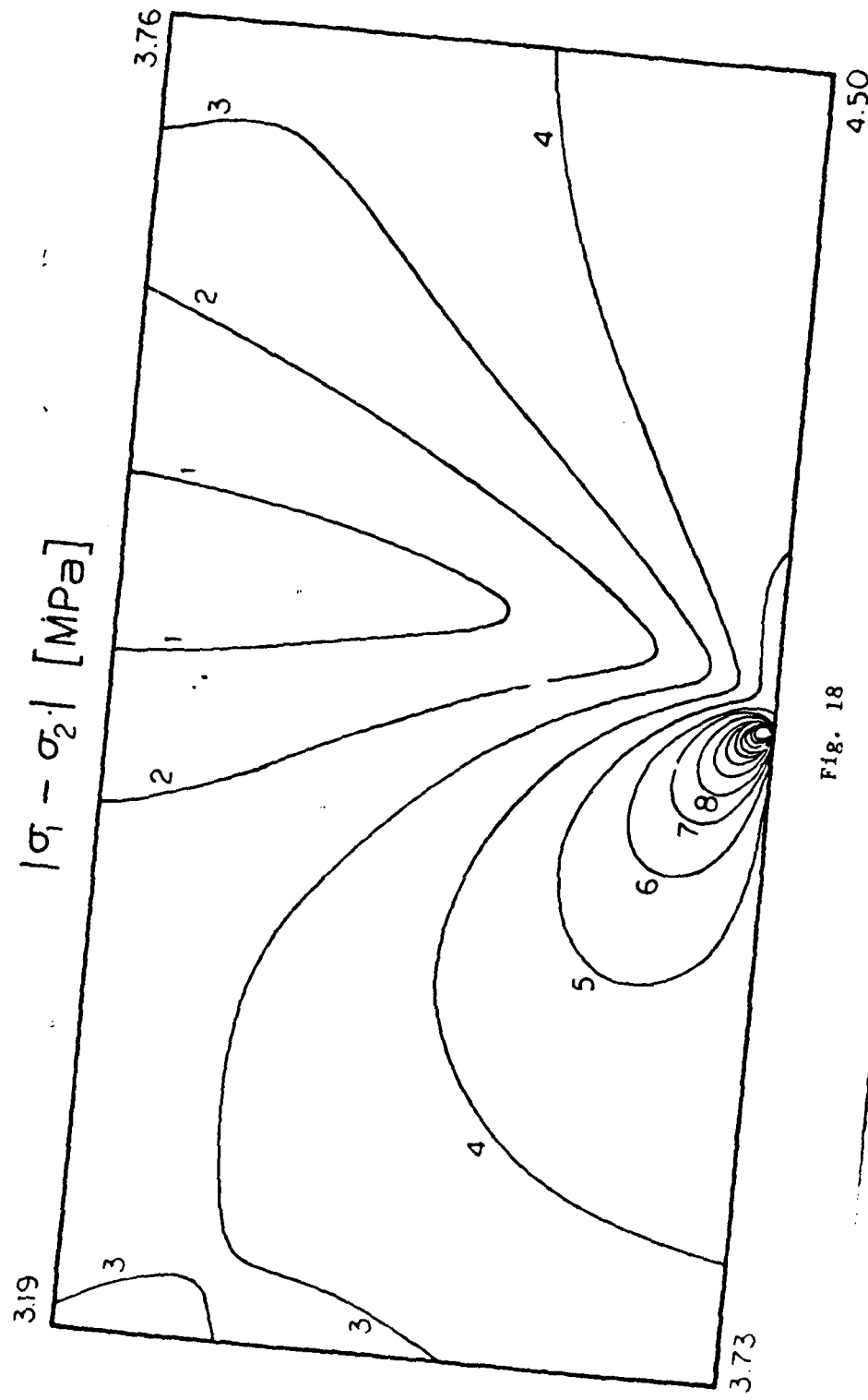


Fig. 18

RDCB No.4 Specimen       $K_I = 1.119 \text{ MNm}^{-1.5}$   
Application Phase       $\bar{\zeta} = 176.7 \text{ mm}$   
Plane Stress       $V = 313.0 \text{ m/sec}$   
 $t = 300 \mu\text{sec}$

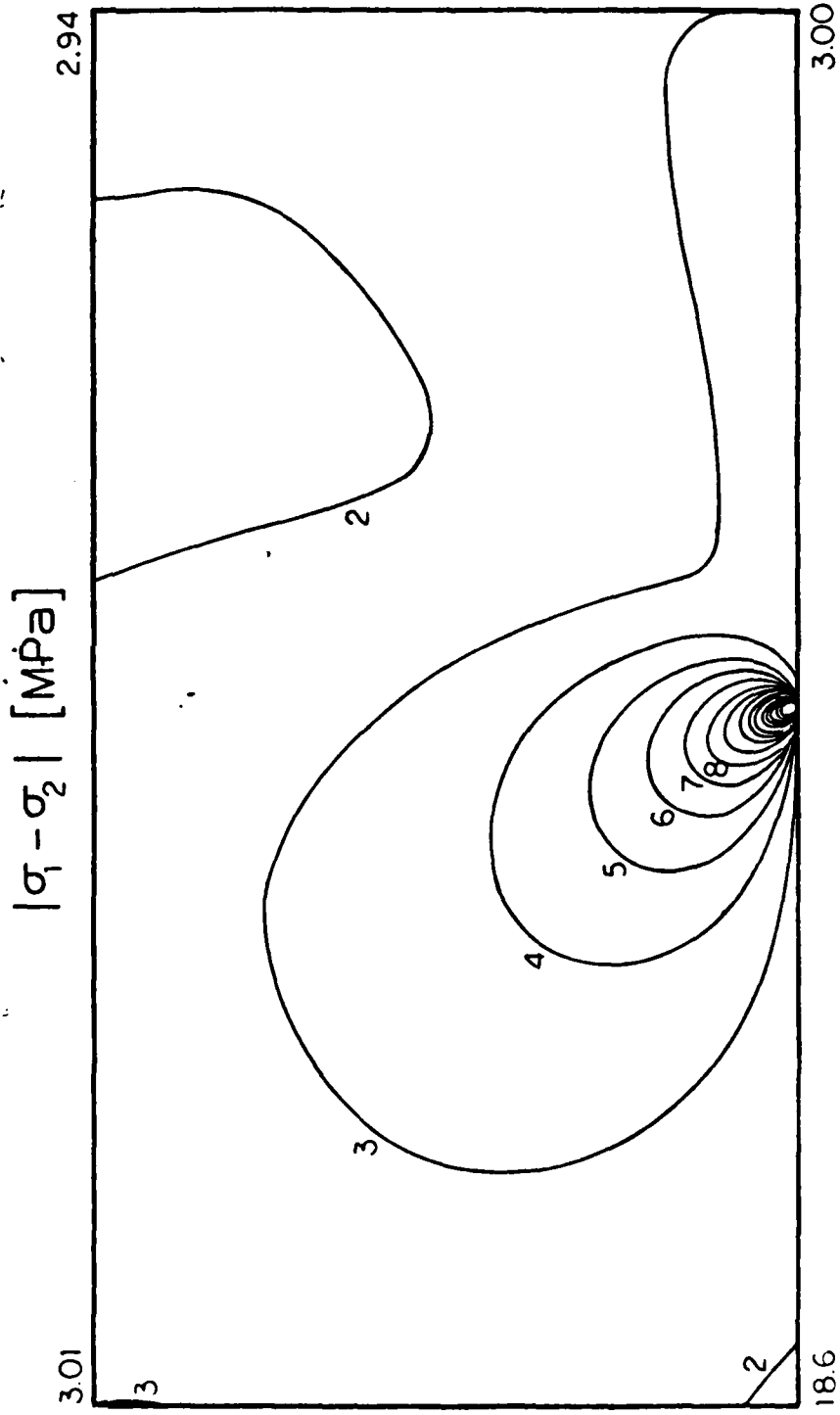


Fig. 19

RDCB No4 Specimen  
 Application Phase  
 Plane Stress  
 $K_I = 0.814 \text{ MNm}^{-1.5}$   
 $\Sigma = 204.0 \text{ mm}$   
 $V = 209.6 \text{ m/sec}$   
 $t = 400 \mu\text{sec}$

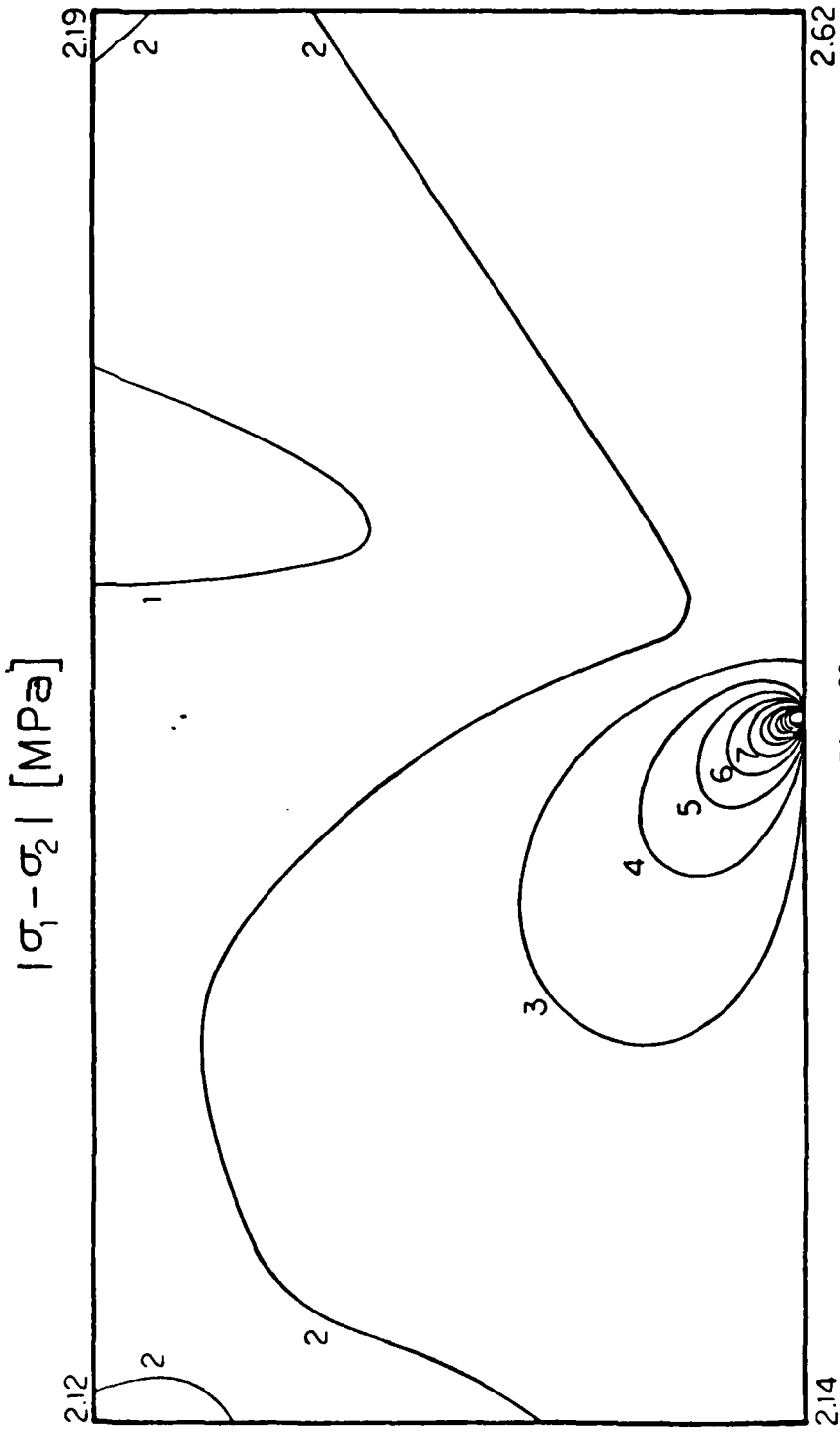


Fig. 20

RDGB No.4 Specimen  
 Application Phase  
 Plane Stress  
 $K_I = 0.701 \text{ MNm}^{-1.5}$   
 $\Delta = 217.2 \text{ mm}$   
 $V = 0.0 \text{ m/sec}$   
 $t = 528.0 \mu\text{sec}$

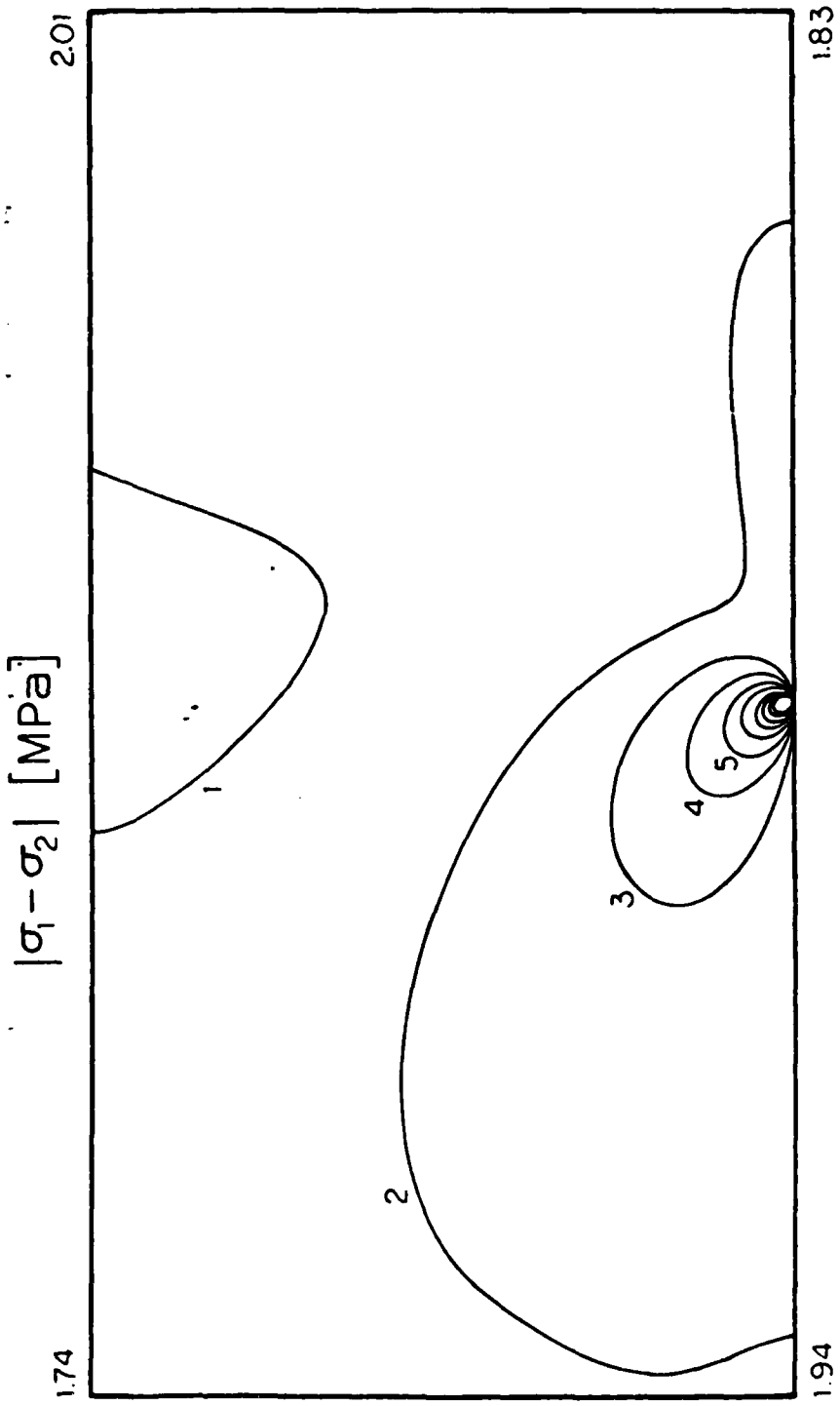


Fig. 21

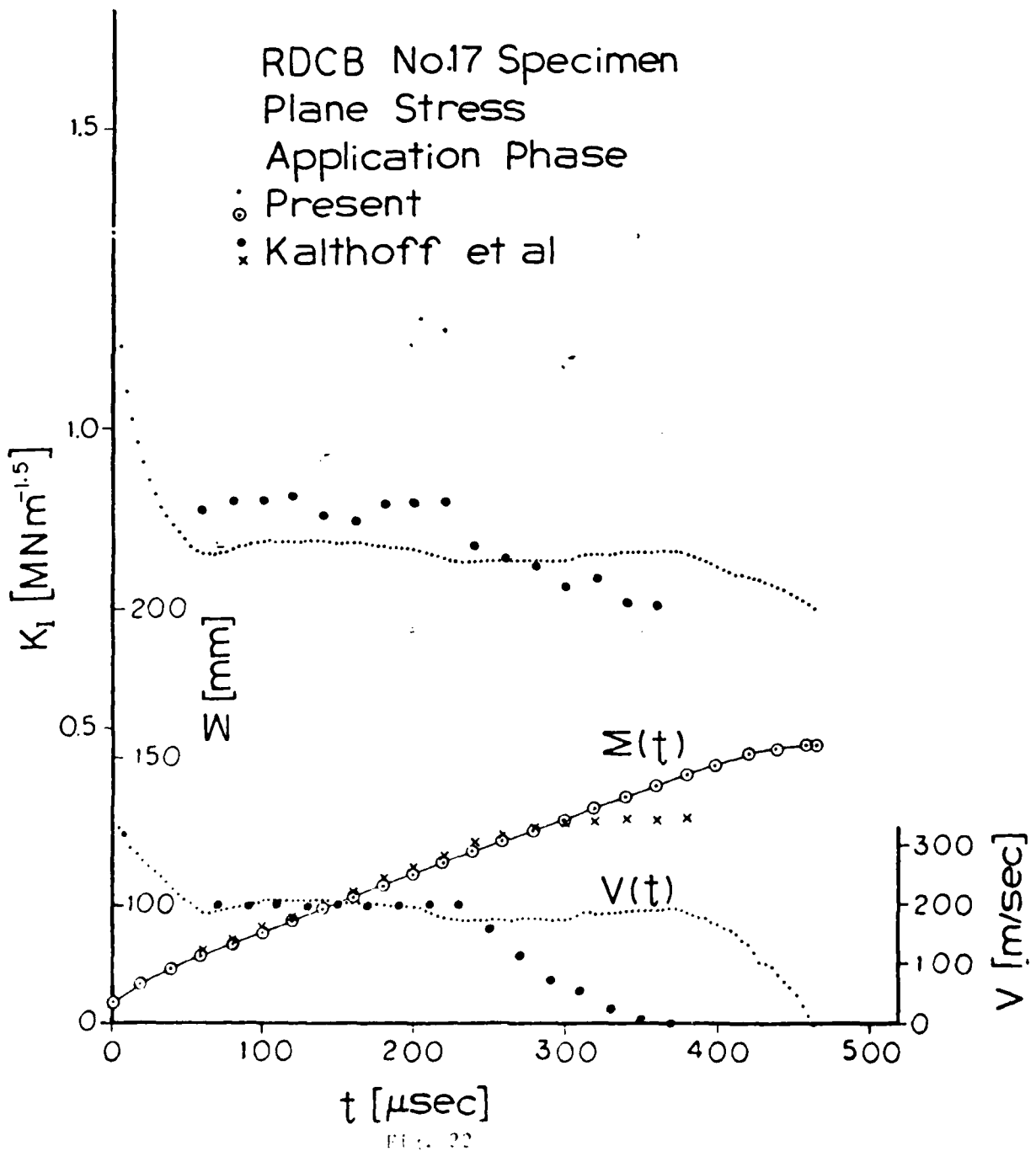


Fig. 22

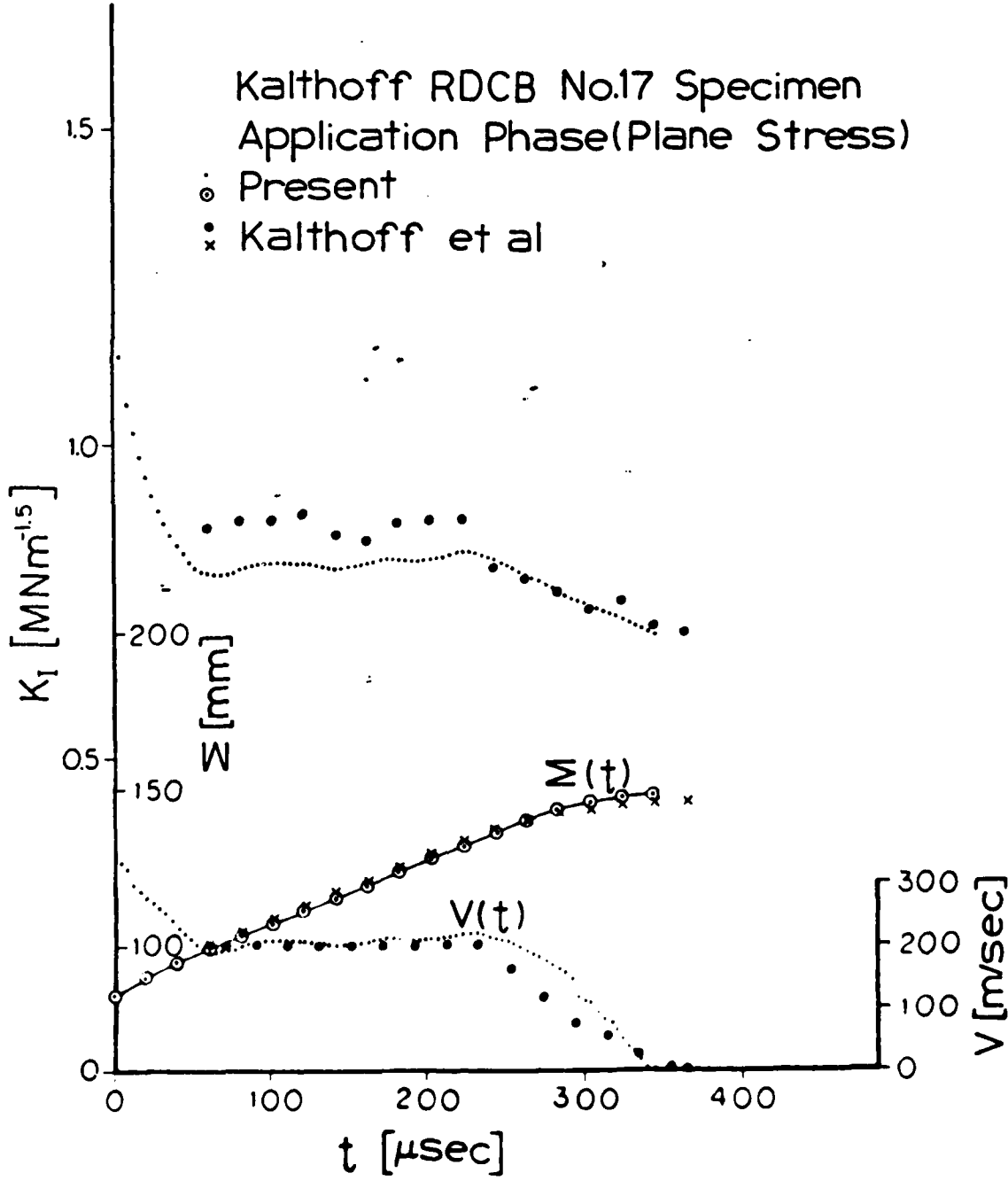


Fig. 23

R D C B  
KALTHOFF No.17 SPECIMEN

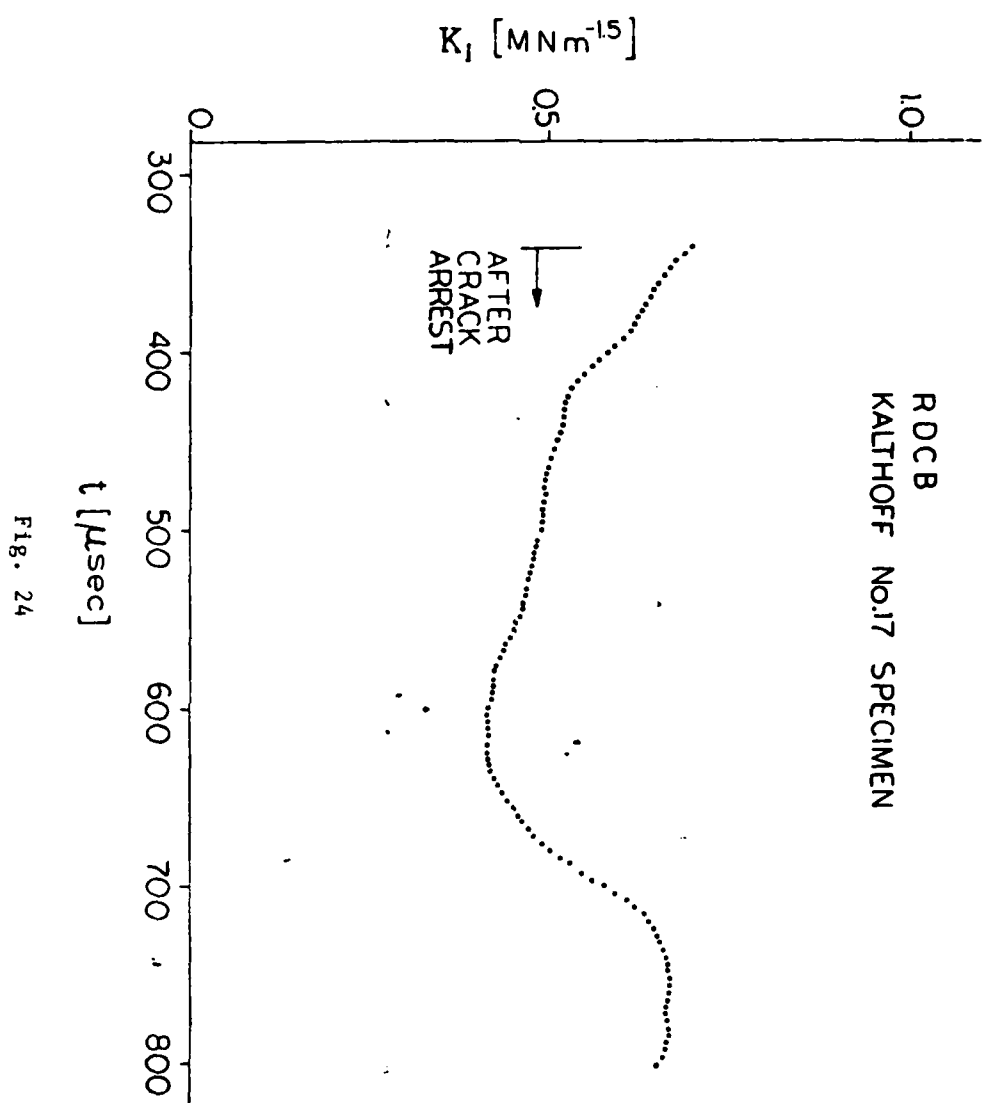


Fig. 24

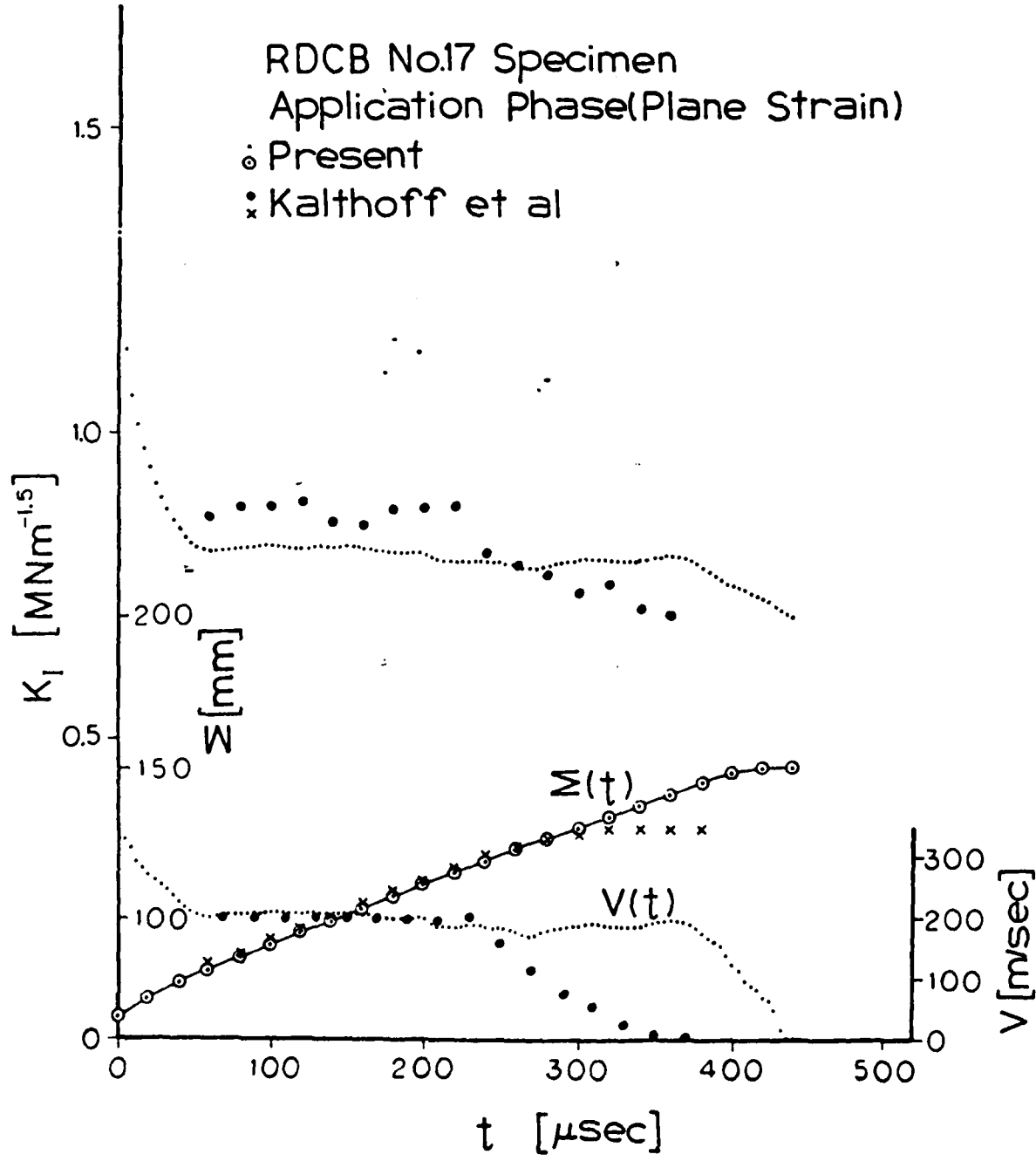


Fig. 25

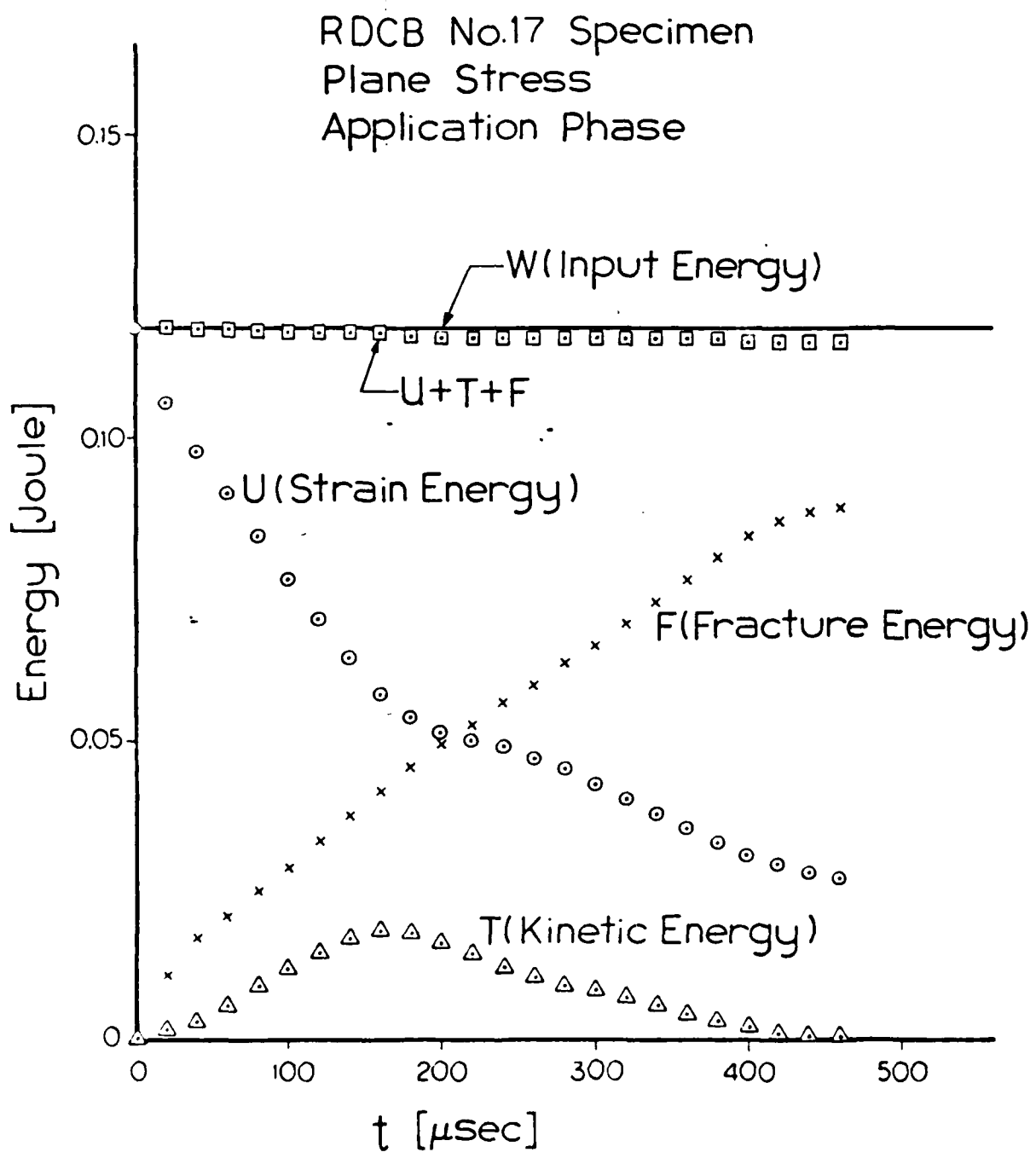


Fig. 26

RDCB No.17 Specimen  
Plane Stress  
Application Phase

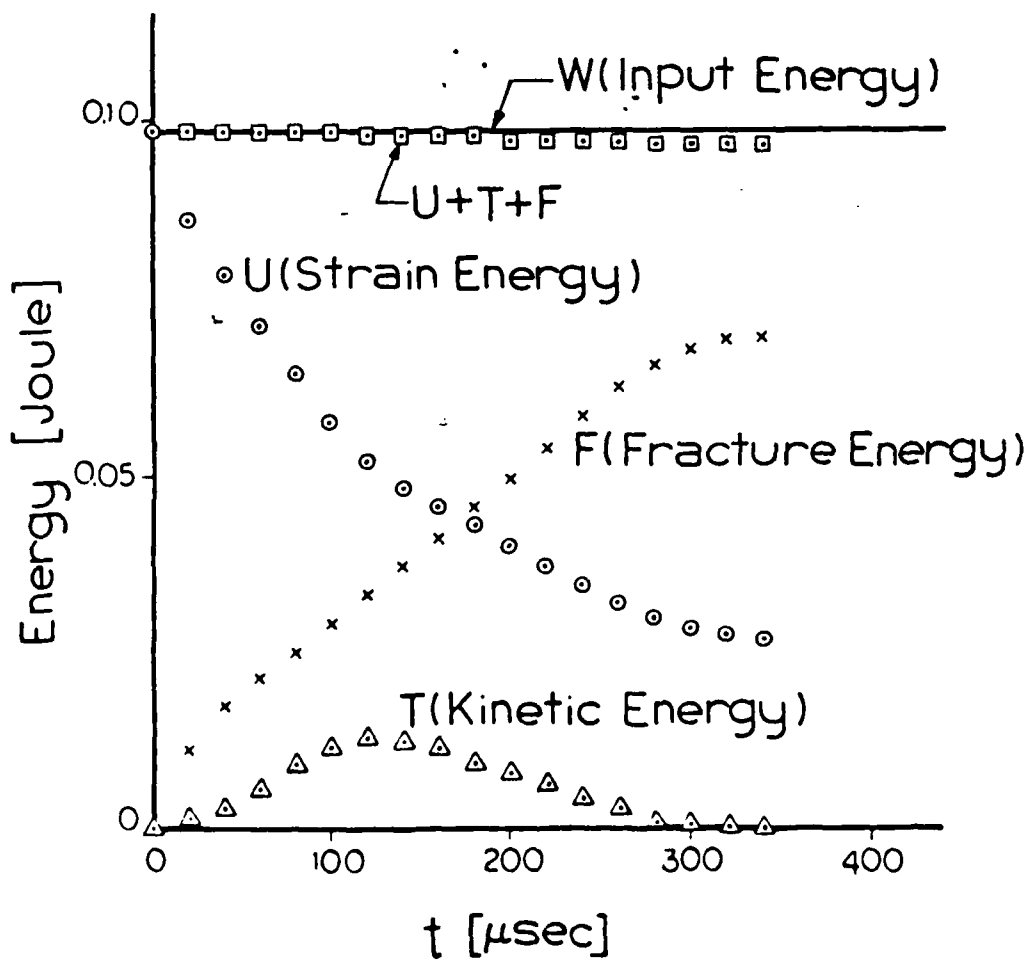


Fig. 27

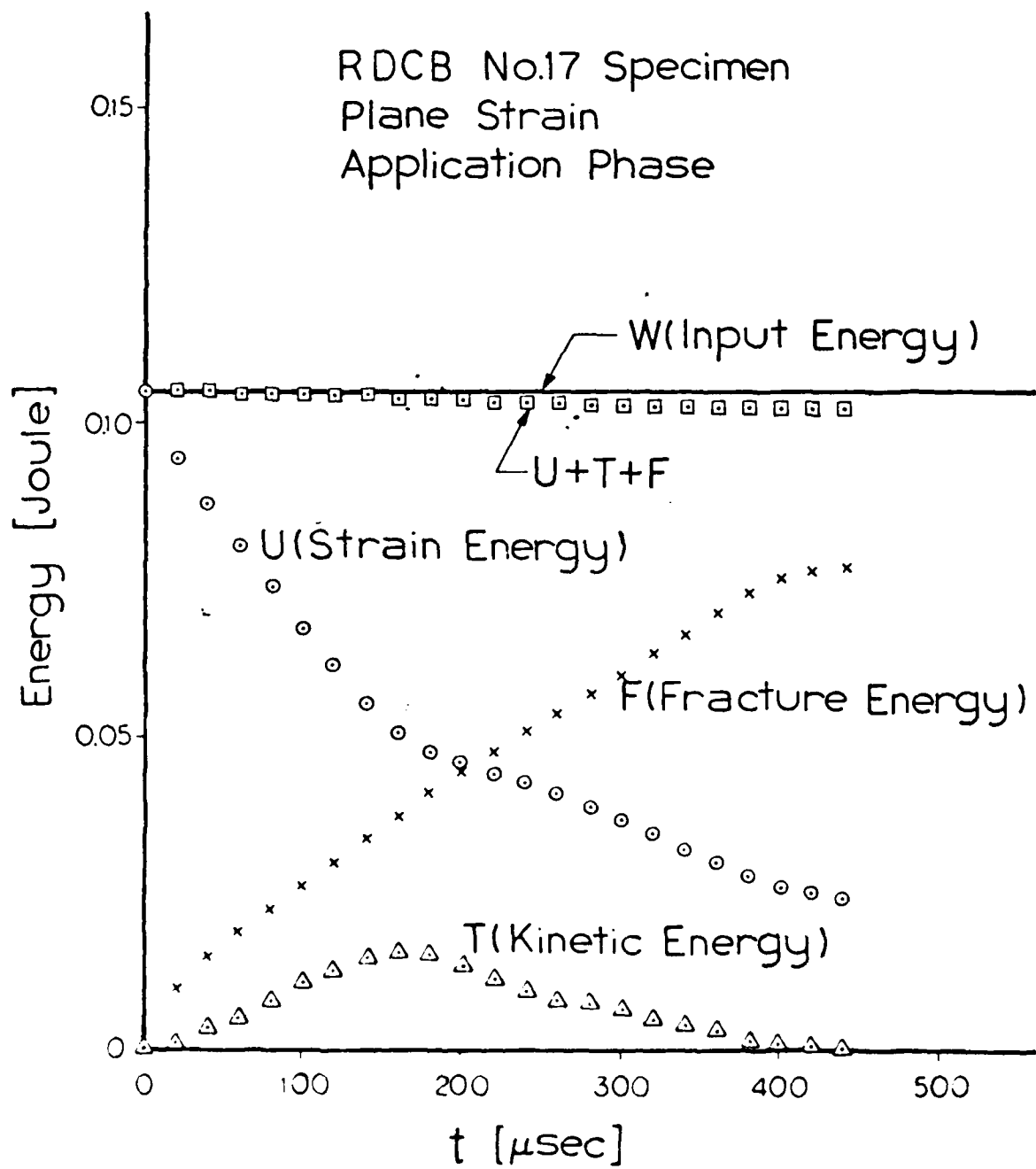


Fig. 28

R DCB No.17 Specimen  
Application Phase  
Plane Stress

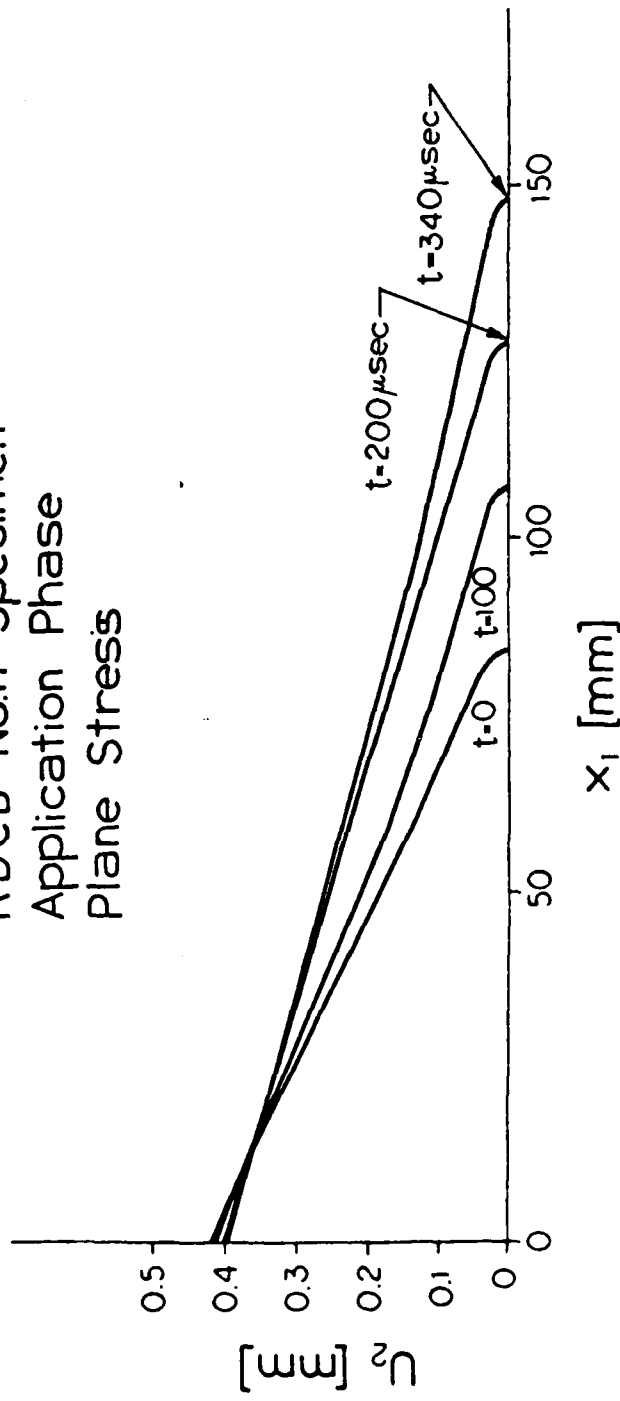
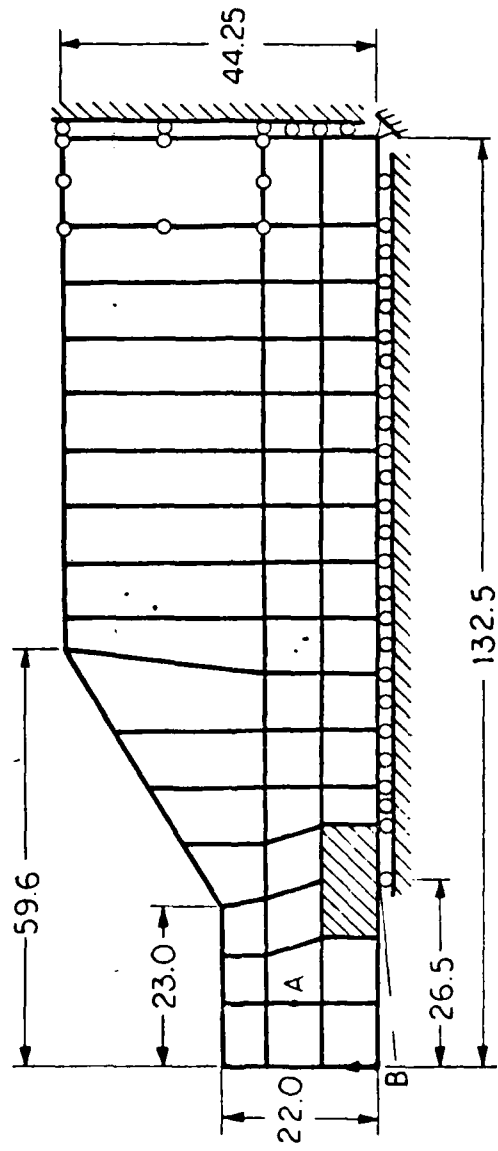


Fig. 29

TDCB Specimen



Thickness  $h=10$  mm  
Dimensions in mm

Fig. 30

TDCB

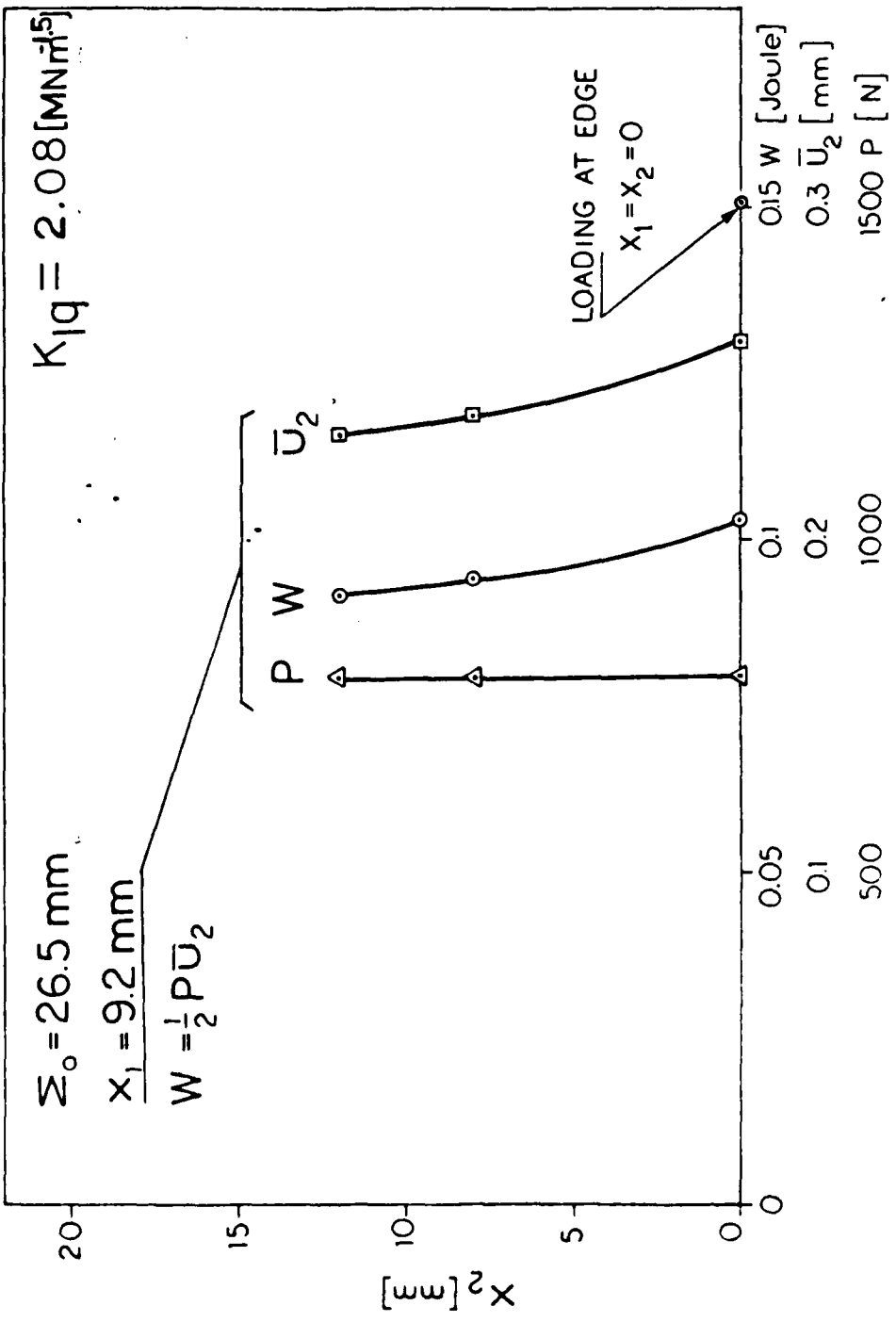
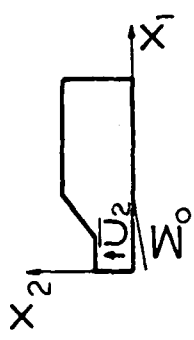


Fig. 31

TDCB (Loading point B)

$\vdots$  Present  
 $\times$  Kalthoff et al (Experimental Results)  
 $\blacksquare$  Kabayashi

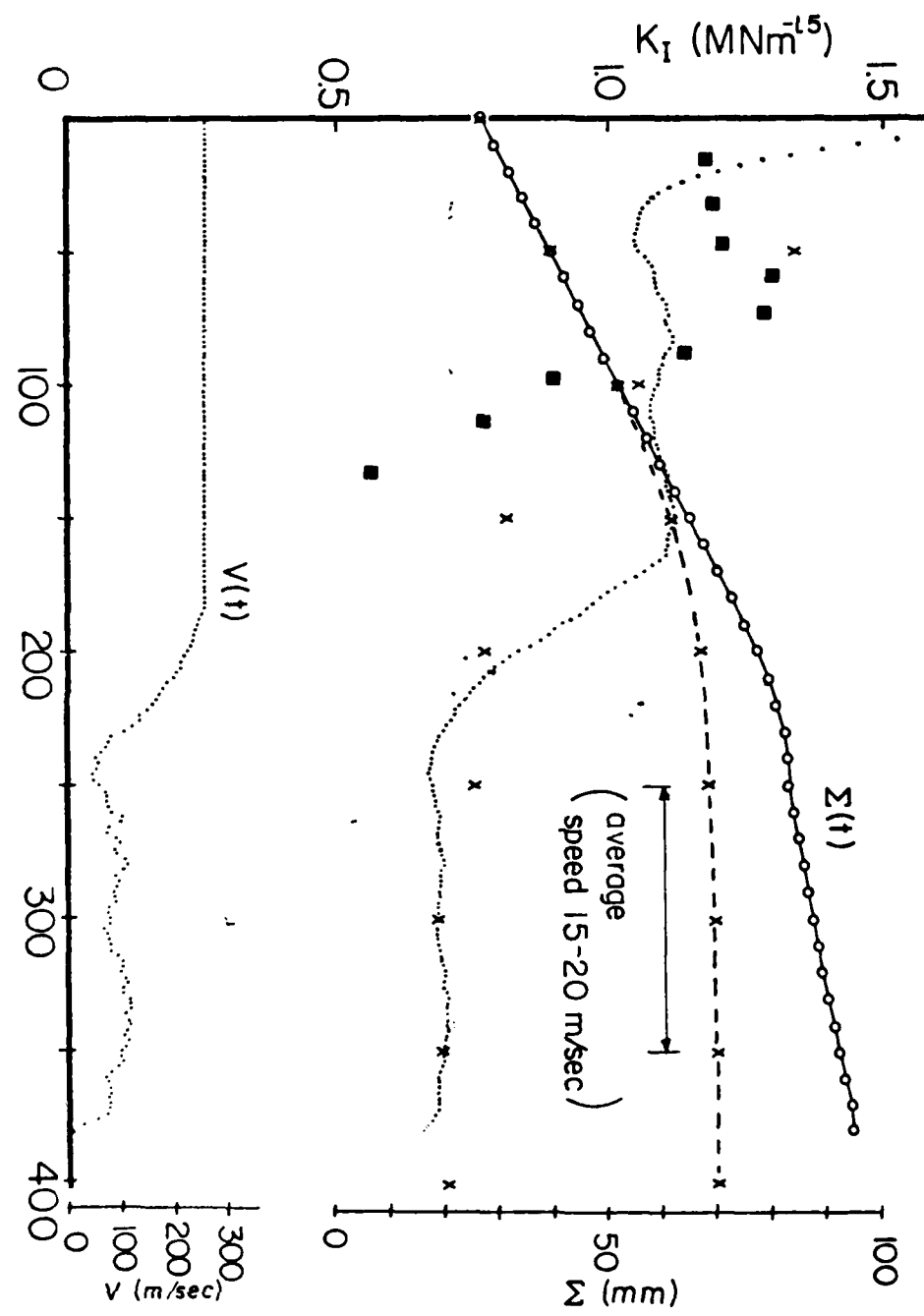
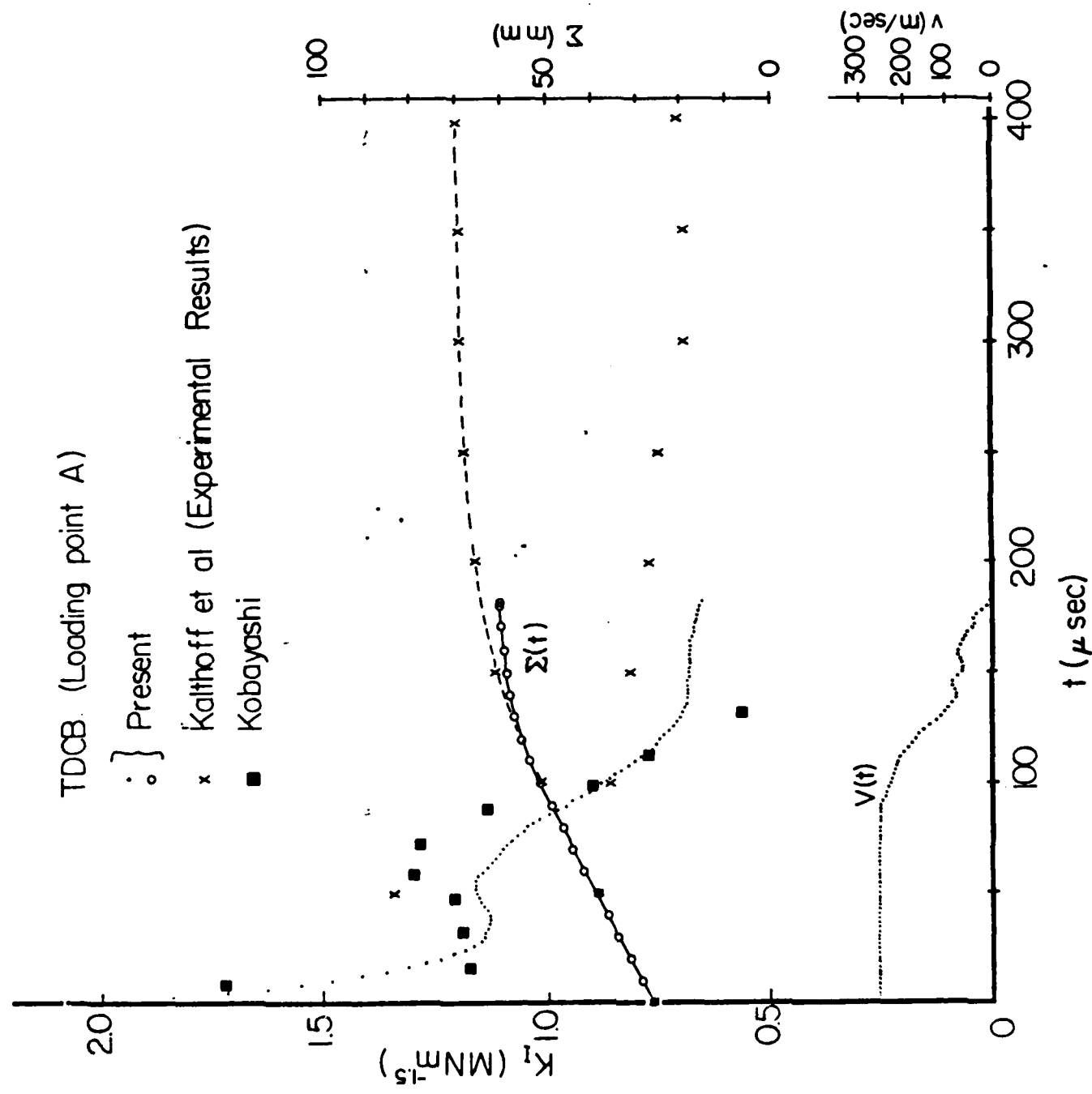


FIG. 32



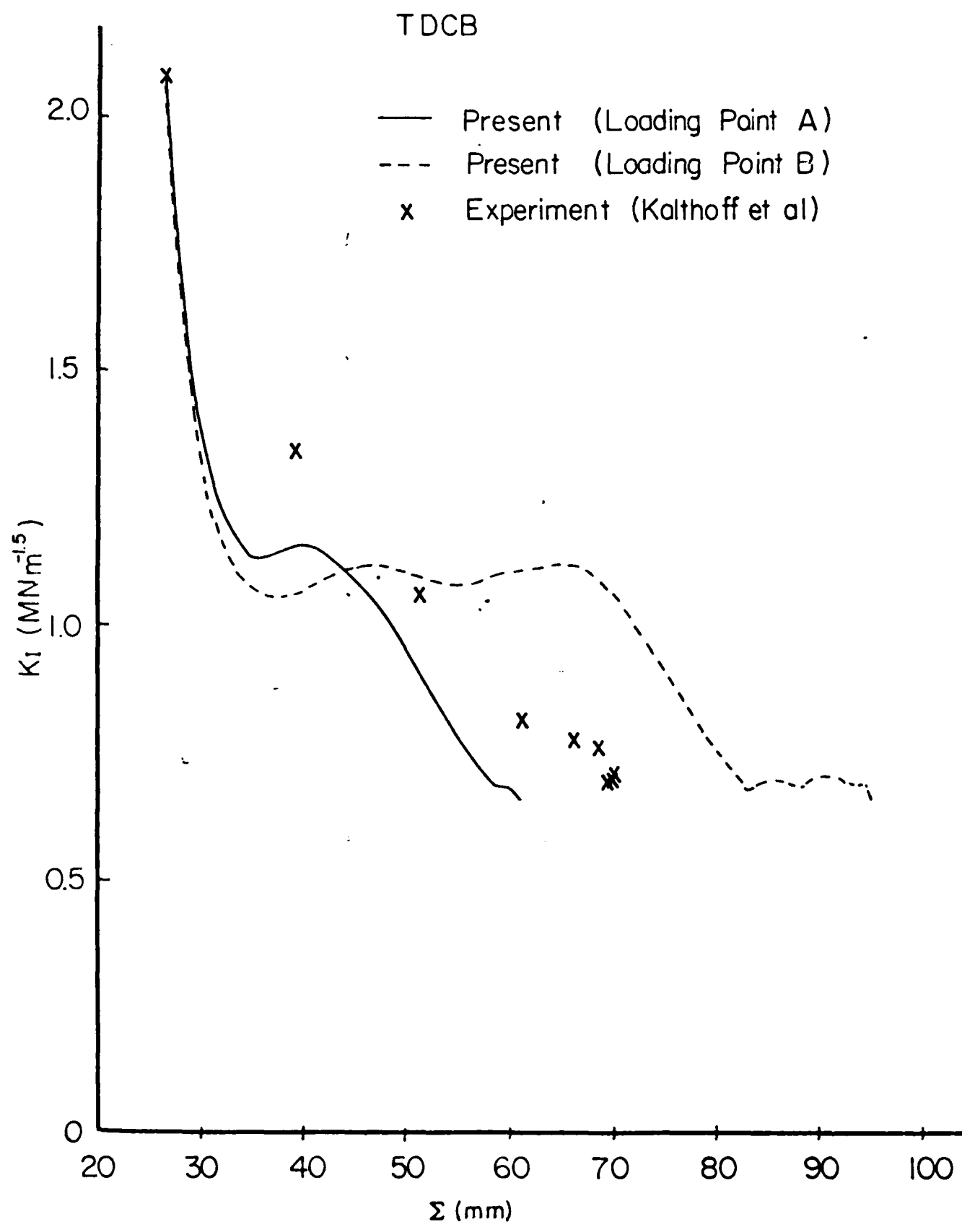
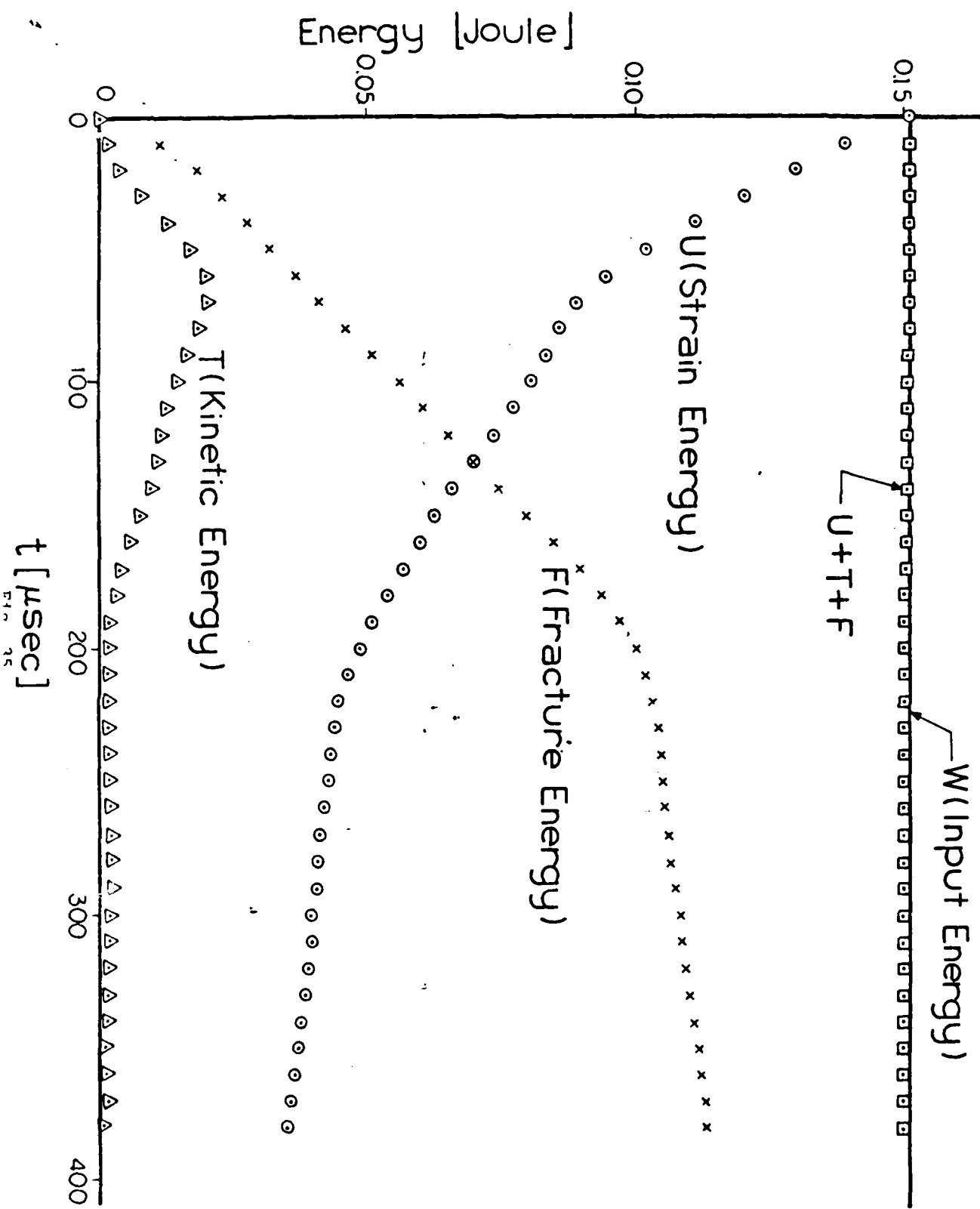
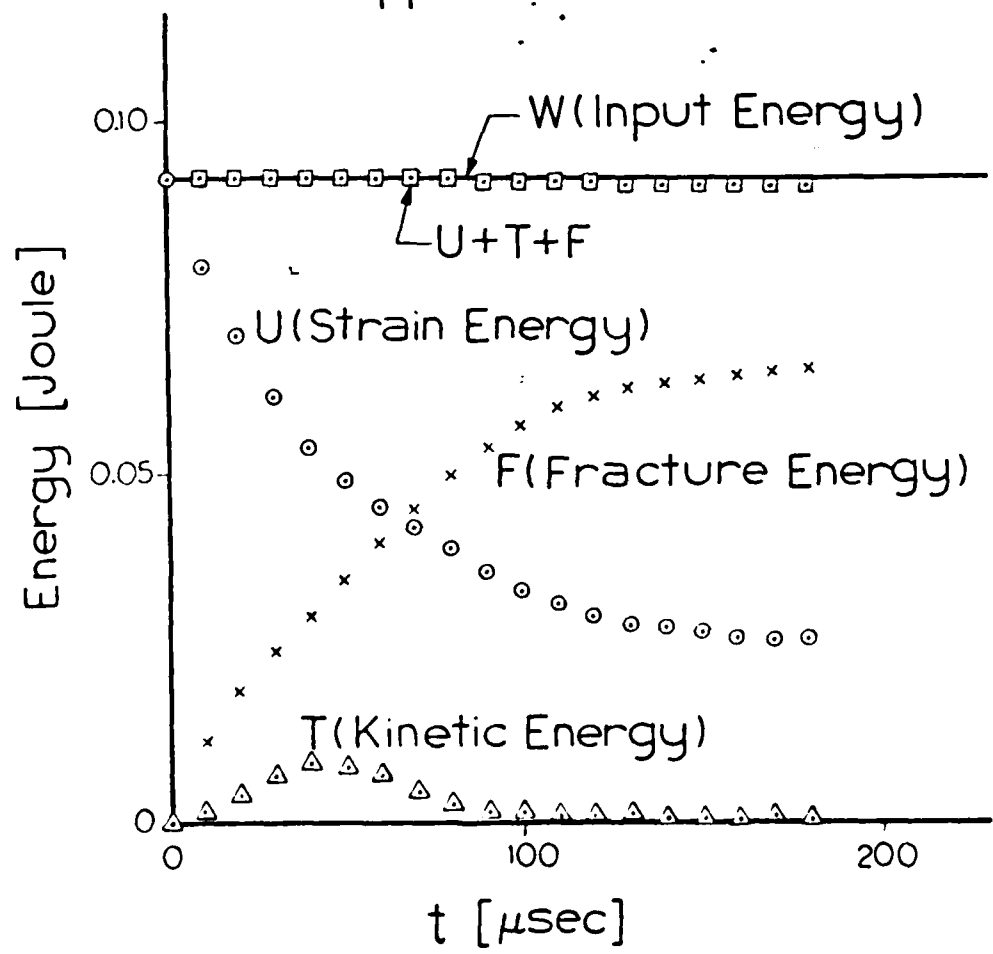


Fig. 34

TDCB Specimen  
Application Phase



TDCB Specimen  
Application Phase



TDCB  
Application Phase  
Plane Stress

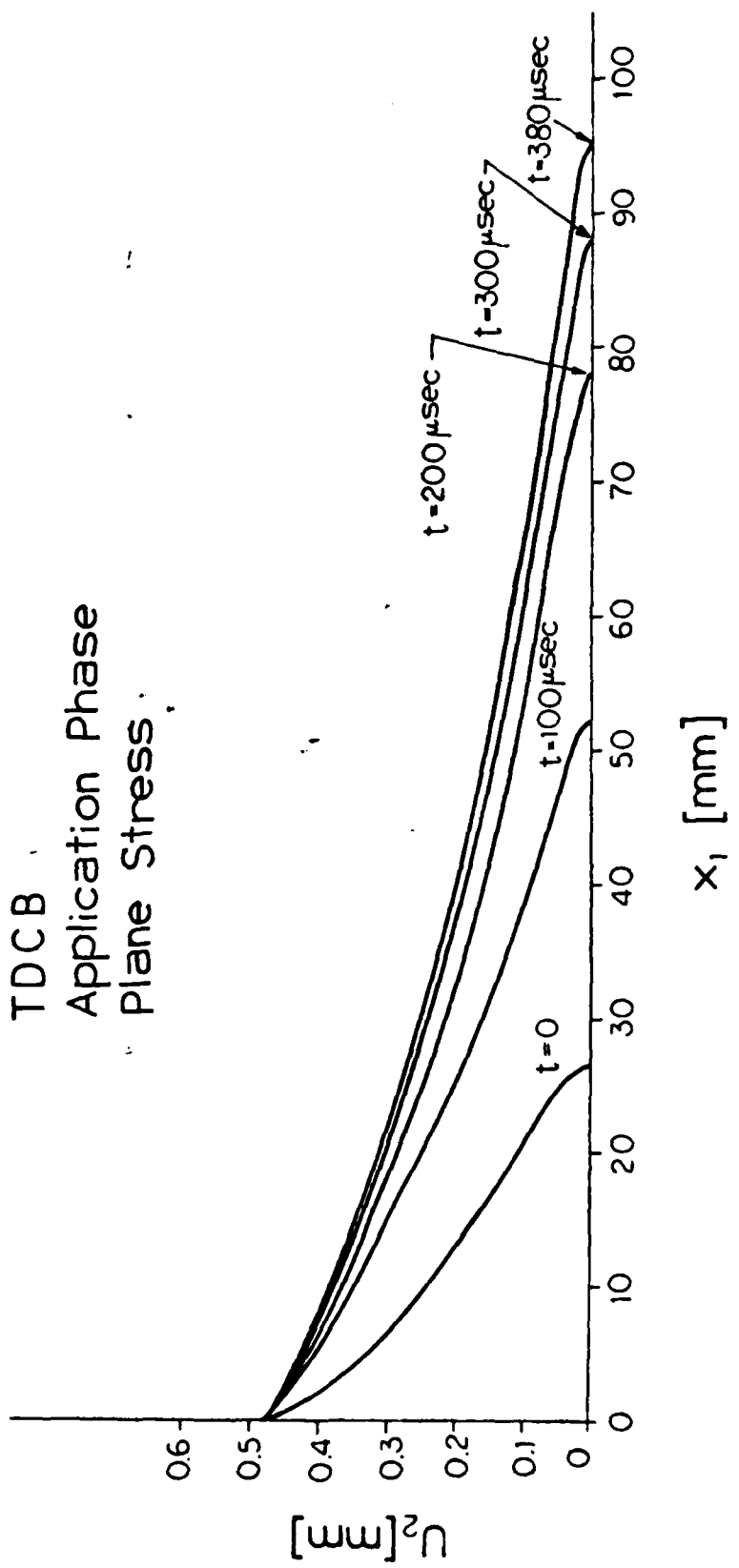


Fig. 37

TDCB Specimen  
Application Phase

$K_I = 2.08 \text{ MNm}^{-1.5}$   
 $\Sigma = 26.5 \text{ mm}$   
 $V = 0.0 \text{ m/sec}$   
 $t = 0.0 \mu\text{sec}$   
 $8 \text{ mm} \times 16 \text{ mm}$

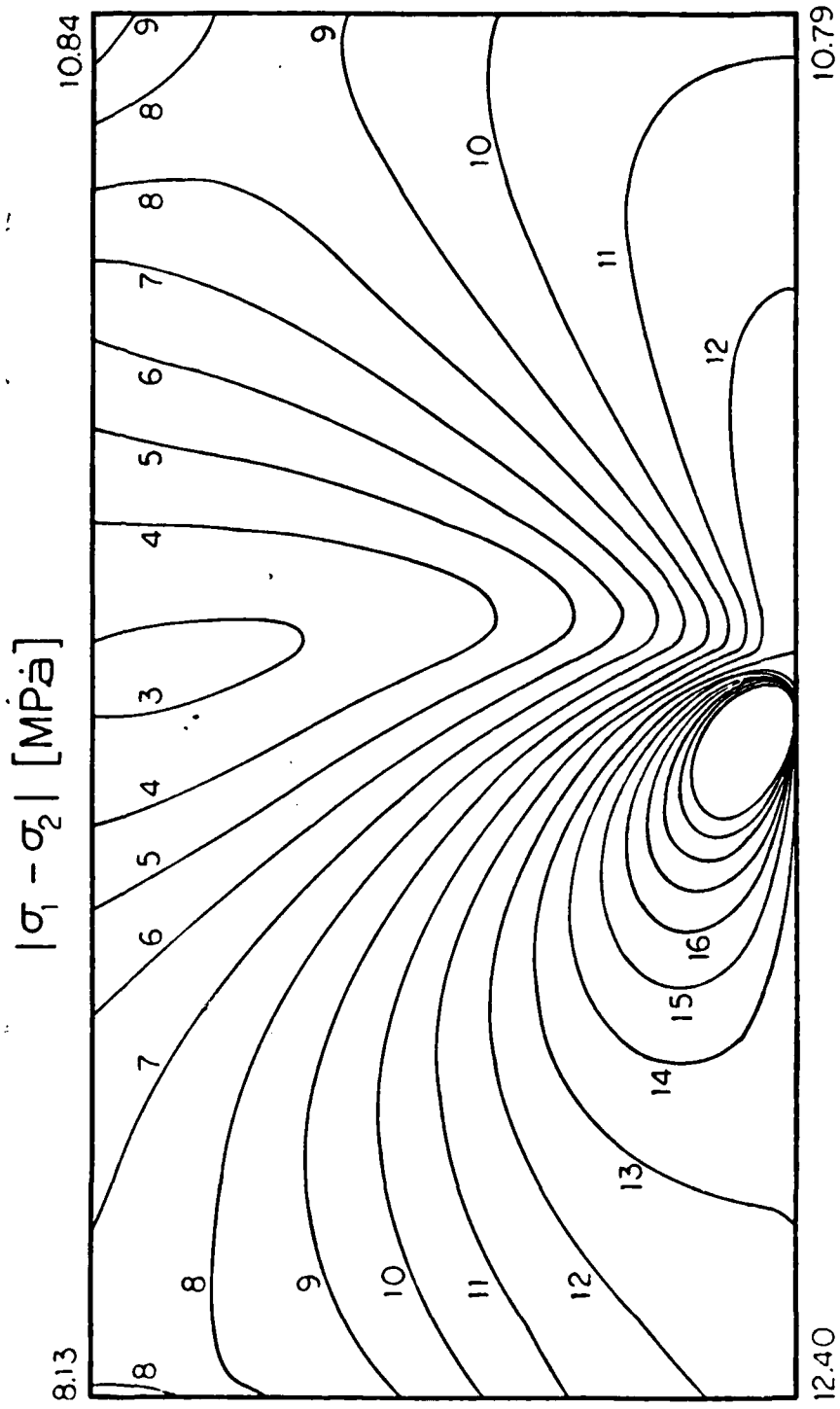


Fig. 38

TDCB Specimen  
 Application Phase  
 $K_I = 1.091 \text{ MNm}^{-1.5}$   
 $\Sigma = 52.0 \text{ mm}$   
 $V = 255.0 \text{ m/sec}$   
 $t = 100.0 \mu\text{sec}$

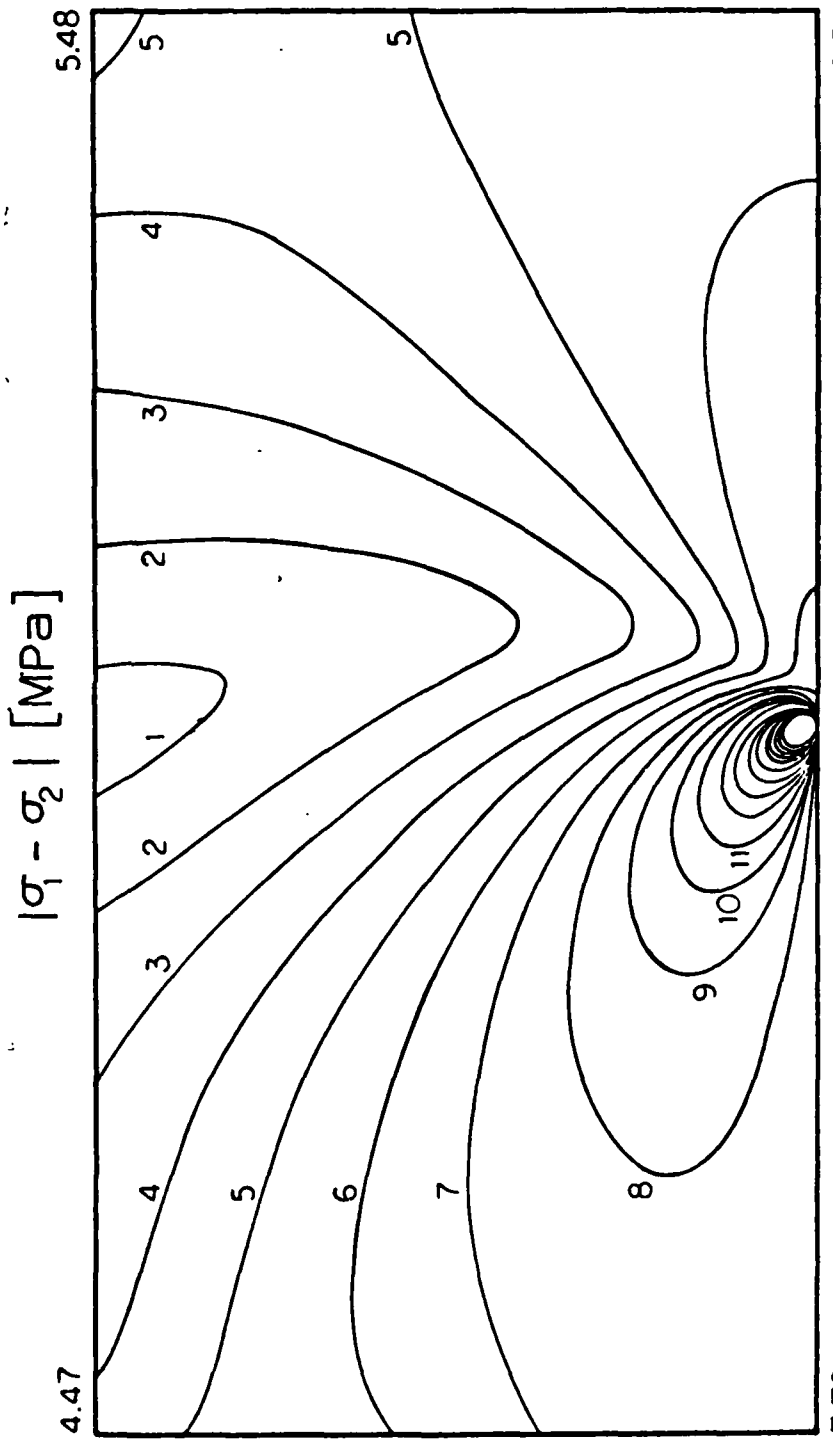


Fig. 39

TDCB Specimen  
Application Phase

$K_I = 0.686 \text{ MNm}^{-1.5}$   
 $\zeta = 87.7 \text{ mm}$   
 $V = 76.4 \text{ m/sec}$   
 $t = 300 \mu\text{sec}$

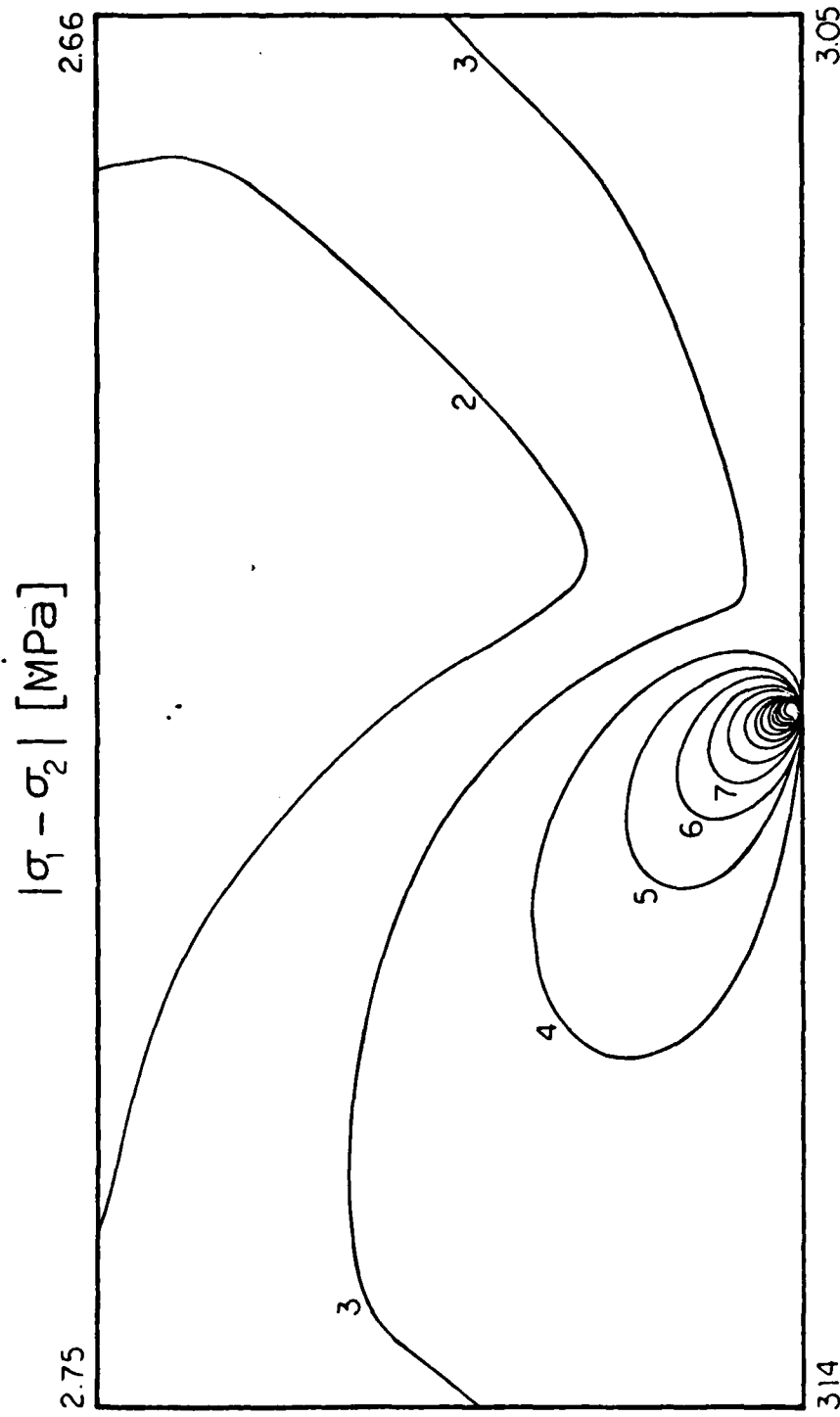


Fig. 41

TDCB Specimen  
Application Phase

$K_I = 0.836 \text{ MNm}^{-1.5}$   
 $\Sigma = 77.2 \text{ mm}$   
 $V = 220.9 \text{ m/sec}$   
 $t = 200 \mu\text{sec}$

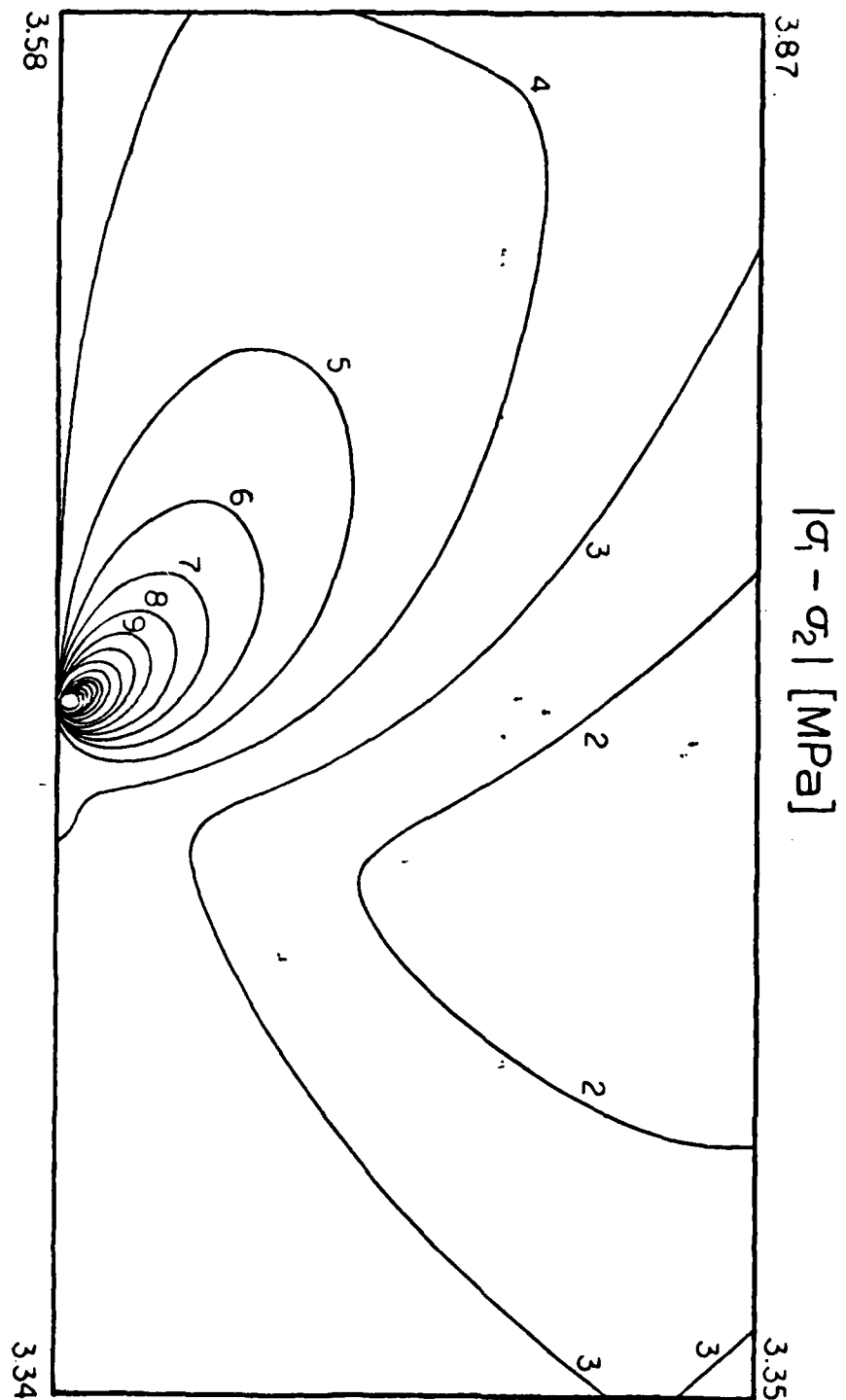
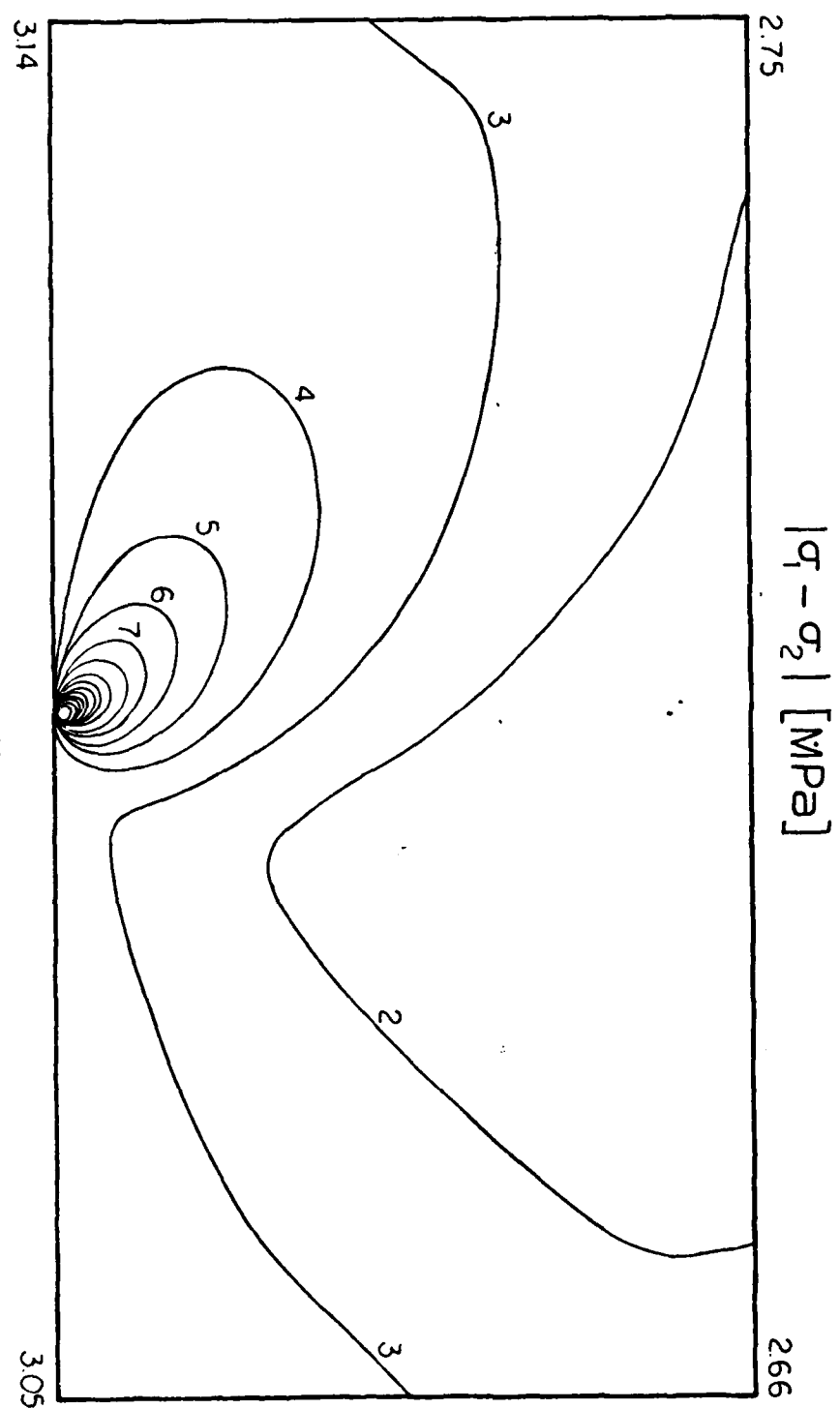


Fig. 40

TDCB Specimen  
Application Phase  
 $K_I = 0.686 \text{ MNm}^{-1.5}$   
 $\Sigma = 87.7 \text{ mm}$   
 $V = 76.4 \text{ m/sec}$   
 $t = 300 \mu\text{sec}$



TDCB Specimen  
Application Phase  
 $K_I = 0.656 \text{ MNm}^{-1.5}$   
 $\Sigma = 94.8 \text{ mm}$   
 $V = 0.0 \text{ m/sec}$   
 $t = 380 \mu\text{sec}$

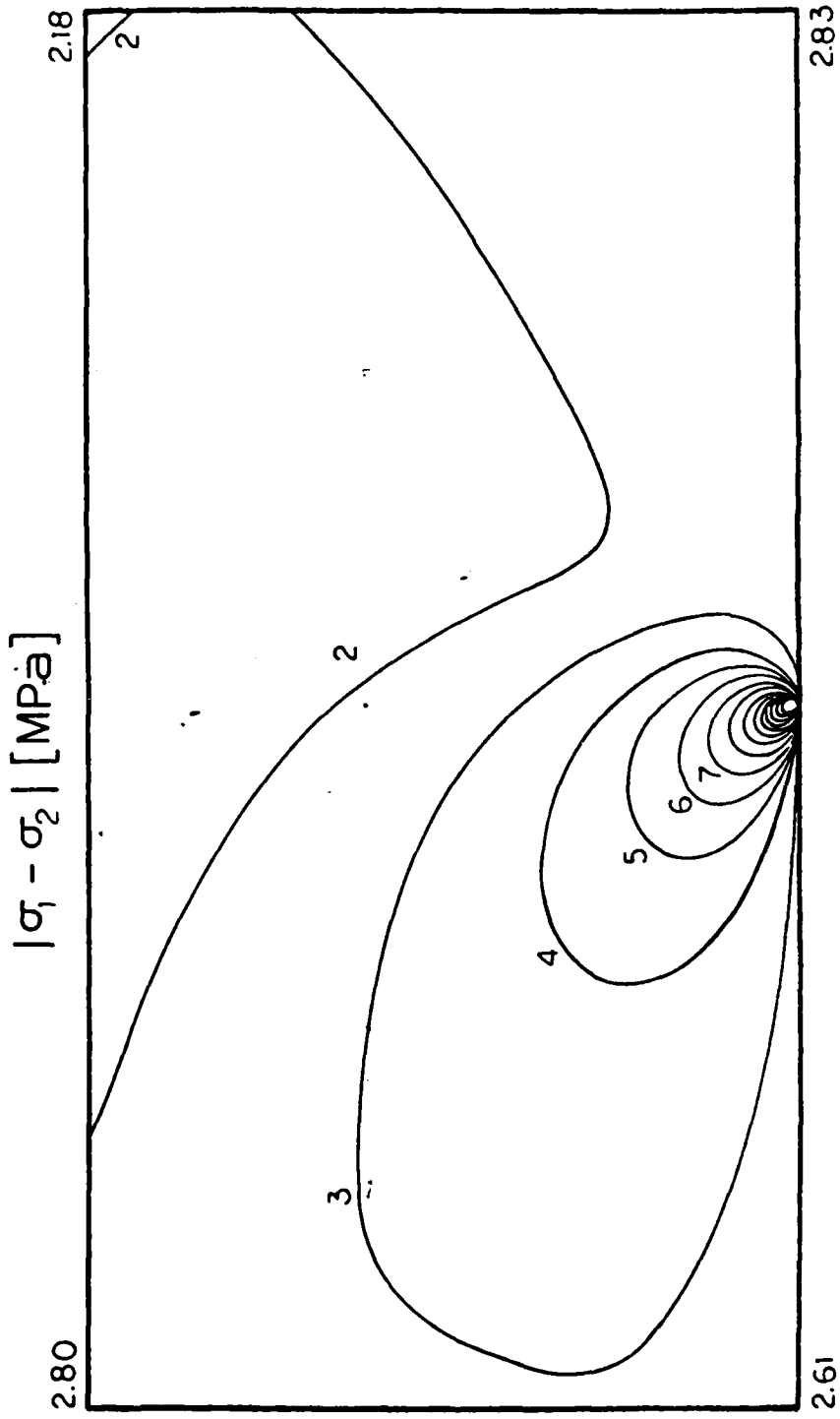


Fig. 4.2

REPORT DOCUMENTATION PAGE		READ INSTRUCTIONS BEFORE COMPLETING FORM
1. REPORT NUMBER 81-GIT-CACM-SNA-9	2. GOVT ACCESSION NO. <i>AD-A103078</i>	3. RECIPIENT'S CATALOG NUMBER
4. TITLE (and Subtitle) Numerical Analysis of Dynamic Crack Propagation Generation and Prediction Studies		5. TYPE OF REPORT & PERIOD COVERED Interim Report
		6. PERFORMING ORG. REPORT NUMBER 81-GIT-CACM-SNA-9
7. AUTHOR(s) T. Nishioka, S.N. Atluri		8. CONTRACT OR GRANT NUMBER(s) N00014-78-C-0636
9. PERFORMING ORGANIZATION NAME AND ADDRESS GIT - Center for the Advancement of Computational Mechanics, School of Civil Engineering Atlanta, GA 30332		10. PROGRAM ELEMENT, PROJECT, TASK AREA & WORK UNIT NUMBERS NR064-610
11. CONTROLLING OFFICE NAME AND ADDRESS Office of Naval Research Structural Mechanics Program Dept. of Navy, Arlington, VA 22217		12. REPORT DATE July 1981
14. MONITORING AGENCY NAME & ADDRESS (if different from Controlling Office)		13. NUMBER OF PAGES 65
		15. SECURITY CLASS. (of this report) Unclassified
		15a. DECLASSIFICATION DOWNGRADING SCHEDULE
16. DISTRIBUTION STATEMENT (of this Report) Unlimited		
17. DISTRIBUTION STATEMENT (of the abstract entered in Block 20, if different from Report)		
18. SUPPLEMENTARY NOTES		
19. KEY WORDS (Continue on reverse side if necessary and identify by block number)		
20. ABSTRACT (Continue on reverse side if necessary and identify by block number) Results of "generation" (determination of dynamic stress-intensity factor variation with time, for a specified crack-propagation history) studies, as well as "prediction" (determination of crack-propagation history for specified dynamic fracture toughness versus crack-velocity relationships) studies of dynamic crack propagation in plane-stress/strain situations are presented and discussed in detail. These studies were conducted by using a transient finite element method wherein the propagating stress-singularity near the propagating crack-tip have been accounted for. Details of numerical procedures for both		

SECURITY CLASSIFICATION OF THIS PAGE(When Data Entered)

the generation and prediction calculations are succinctly described. In both the generation and prediction studies, the present numerical results are compared with available experimental data. It is found that the important problem of dynamic crack propagation prediction can be accurately handled with the present procedures.

SECURITY CLASSIFICATION OF THIS PAGE(When Data Entered)